TECHNISCHE UNIVERSITÄT WIEN
Vienna | Austria

Master Thesis

Restoring Complex Langevin Convergence with Lefschetz Thimble-Based Density Modifications

Carried out for the purpose of obtaining the academic degree of Diplom-Ingenieur (Dipl.-Ing or DI)

Fabian Helmberger, BSc

submitted at
Technical University Vienna
Faculty of Physics
Institute for Theoretical Physics

Supervision: Privatdoz. Dr.rer.nat. **Kirill Boguslavski**
Dipl.-Ing. **Paul Hotzy**, BSc BSc
Institut for Theoretical Physics
Technical University of Vienna
Wiedner Hauptstr. 8–10, 1040 Wien, Österreich

Wien, im May 2025

Die approbierte gedruckte Originalversion dieser Diplomarbeit ist an der TU Wien Bibliothek verfügbar
The approved original version of this thesis is available in print at TU Wien Bibliothek.
TU Bibliothek Your knowledge hub

Kurzfassung

Die Komplexe Langevin (CL)-Methode ist ein vielversprechender Ansatz zur Überwindung des *sign problem* in Monte-Carlo-Integrationen, die zur Berechnung von Observablen in Quantenfeldtheorien mit komplexer Wirkung verwendet werden. In dieser Arbeit untersuchen wir ein null-dimensionales skalares Modell mit ϕ^4-Wechselwirkung und stellen fest, dass CL nur in bestimmten Bereichen der symmetrischen Phase korrekte Ergebnisse liefert. Um auch außerhalb dieser Bereiche und insbesondere in der gebrochenen Phase eine korrekte Konvergenz wiederherzustellen, zeigen wir, dass eine Methode, die zuvor erfolgreich auf Modelle mit kompakten Definitionsbereichen angewendet wurde, durch einfache Modifikationen auch auf den Fall nicht-kompakter Definitionsbereiche übertragen werden kann. Dieser additive Gewicht-Regularisierungsansatz verändert die zugrunde liegende Lefschetz-Thimble-Struktur der Theorie. Für eine geeignete Wahl der Modifikationsparameter zeigen wir, dass diese Methode die Konvergenzeigenschaften von CL auch in der gebrochenen Phase verbessern kann. Unsere numerischen Ergebnisse stützen die Vermutung, dass die korrekte Konvergenz der CL-Methode eine Thimble-Struktur mit nur einem relevanten Beitrag erfordert. Diese Erkenntnisse könnten den Weg für die Anwendung von CL in Kombination mit einer Dichte-Modifikation auf höherdimensionale Theorien mit nicht-kompakten Definitionsbereichen ebnen und so die Zuverlässigkeit der Methode in diesen Kontexten potenziell verbessern. Weitere Untersuchungen sind erforderlich, um diese Methode im feldtheoretischen Kontext anzuwenden.

Die approbierte gedruckte Originalversion dieser Diplomarbeit ist an der TU Wien Bibliothek verfügbar
The approved original version of this thesis is available in print at TU Wien Bibliothek.

Abstract

The Complex Langevin (CL) method is a promising candidate for overcoming the sign problem in Monte Carlo integrations used to calculate observables in quantum field theories with a complex action. In this work, we investigate a zero-dimensional scalar model with ϕ^4 interaction and observe that CL yields correct results only in certain regimes of the symmetric phase. To restore correct convergence beyond these regimes, and in particular, in the broken phase, we show that a method successfully applied to models defined on compact domains can be extended to the considered case of non-compact domains using simple modifications. This additive weight regularization approach modifies the underlying Lefschetz thimble structure of the theory. For a given choice of modification parameters, we show that this method can be used to improve the convergence behavior of CL even in the phase of broken symmetry. Our numerical results support the conjecture that the correct convergence of the CL method requires a single-thimble structure. These findings may pave the way for applying CL in combination with a density modification to higher-dimensional theories on non-compact domains, potentially improving the reliability of CL in these circumstances. Further research is needed to apply this method in a field-theoretic context.

Die approbierte gedruckte Originalversion dieser Diplomarbeit ist an der TU Wien Bibliothek verfügbar
The approved original version of this thesis is available in print at TU Wien Bibliothek.
TU Bibliothek Your knowledge hub WIEN

Acknowledgements

First and foremost, I would like to express my deepest gratitude to my supervisor, Dr. Kirill Boguslavski, for his constant support, insightful guidance, and encouragement during the course of this project. His expertise and thoughtful input were invaluable throughout the development of this work. From the early conceptual stages to the final analyses, his ability to pose the right questions, provide critical feedback, and maintain a clear vision for the project greatly influenced both the direction and the overall quality of this thesis.

I am also grateful to Dr. Paul Hotzy for his valuable feedback and engaging discussions, which not only greatly enhanced my understanding of the topic at hand, but also taught me invaluable lessons in structuring a problem from first principles, translating ideas into efficient code, and approaching implementation step by step with precision and clarity.

A special thanks goes to Dr. David Müller for his highly impactful contributions to the project—his technical insights and thoughtful suggestions were a significant support throughout various stages of the work. I would also like to thank the members of Dr. Boguslavski's group for providing a stimulating research environment and for many fruitful conversations during my studies.

On a more personal note, I am grateful to my family and friends for their patience, understanding, and moral support over the years. Without their encouragement, this journey would have been much more difficult.

Die approbierte gedruckte Originalversion dieser Diplomarbeit ist an der TU Wien Bibliothek verfügbar
The approved original version of this thesis is available in print at TU Wien Bibliothek.

Contents

Die approbierte gedruckte Originalversion dieser Diplomarbeit ist an der TU Wien Bibliothek verfügbar
The approved original version of this thesis is available in print at TU Wien Bibliothek.

Chapter 1

Introduction

Quantum field theories with complex actions arise in a variety of important physical settings, ranging from quantum chromodynamics at finite chemical potential to real-time dynamics and topological terms in lattice gauge theories [1–6]. In these contexts, conventional Monte Carlo methods face a fundamental obstacle: the infamous sign problem [5, 7]. When the action becomes complex, the probability weight e^{-S} is no longer positive-definite, rendering importance sampling methods unreliable or inapplicable. To address this problem, several alternative approaches have been proposed.

Among the most studied approaches are the complex Langevin (CL) [8, 9] method and the Lefschetz thimble decomposition of the path integral [10–15]. The CL method is based on the concept of stochastic quantization, originally introduced by Parisi and Wu [16], which formulates quantum field theories in terms of a stochastic process. In its complexified version, the method extends the field variables into a complexified field space and evolves them according to a complex stochastic differential equation. In favorable cases, it can provide correct results even in the presence of a severe sign problem. However, the method is not guaranteed to converge correctly and may yield incorrect results due to excursions into regions of complexified field space [17]. On the other hand, the Lefschetz thimble approach provides a geometric reformulation of the path integral. By analytically continuing the fields and deforming the integration contour onto steepest-descent manifolds (thimbles) associated with critical points of the complexified action, one obtains an alternative representation of the theory. Along each thimble, the imaginary part of the action remains constant, and the real part increases steeply away from the critical point. This results in an integral with real and positive weights, circumventing the sign problem in principle. However, practical applications of this method are hindered by the difficulty of determining which thimbles contribute and how to sample them efficiently [15].

Interestingly, similarities between these two methods have been highlighted in recent literature [18–21]. Both are fundamentally connected to the critical points of the complexified action: in the thimble approach, these points are the sources of steepest descent and ascent flows that define the thimbles, while in CL dynamics, critical points correspond to locations where the drift term vanishes, leaving only diffusion. For attractive critical points, the equilibrium distribution in CL tends to remain localized nearby, which has led to the empirical observation that CL may converge correctly when its trajectories stay close to a single relevant thimble [22, 23]. The natural question thus arises: What does the thimble structure tell us about the convergence of CL? This question lies at the heart of this thesis.

Recent studies have made progress in bridging the CL dynamics and the underlying thimble geometry. A notable strategy is the enforcement of a single-relevant thimble structure via density modifications. The authors in [18, 24] investigated such modifications to steer CL trajectories closer to the dominant thimble and found that convergence improves in such cases. A particularly effective and systematic approach has been developed in [21], where the authors propose density modifications that deform the distribution so that stochastic trajectories align with a single relevant compact thimble associated with an attractive critical point. Their method includes a

Die approbierte gedruckte Originalversion dieser Diplomarbeit ist an der TU Wien Bibliothek verfügbar
The approved original version of this thesis is available in print at TU Wien Bibliothek.
TU Bibliothek Your knowledge hub WIEN

bias correction scheme that allows reconstruction of observables from the original theory, ensuring that the modification does not alter physical observables. This framework enables reliable CL simulations in models suffering from a severe sign problem and is demonstrated for theories defined on compact manifolds.

In this thesis, we adapt and extend these ideas to non-compact theories. By studying a zero-dimensional scalar model — a simplified but nontrivial model — we aim to explore the relationship between the convergence behavior of the CL method and the structure of the relevant Lefschetz thimbles. The advantage of working in zero dimensions is that the thimble structure can be analyzed in detail, and exact results can be obtained for comparison. This allows for a controlled investigation into the interplay between complex stochastic dynamics and the analytic properties of the path integral. In particular, we focus on regions of parameter space where the theory undergoes a phase transition and where multiple thimbles become relevant.

We implement a density modification scheme tailored to reduce the number of relevant thimbles to one, thus potentially improving convergence of the CL method. Crucially, we investigate whether the bias introduced by such modifications can be accurately corrected within the CL framework itself. By working in a regime where multiple thimbles become relevant (e.g., near phase transitions), we aim to test the robustness and limitations of this approach and provide further insight into the interplay between stochastic quantization and the analytic structure of path integrals. The central goal is to reveal how thimble geometry guides the convergence behavior of CL dynamics and how targeted modifications can align stochastic flows with single relevant thimbles.

The structure of this thesis is as follows. In Chapter 2, we review the theoretical background of the scalar model under consideration and introduce the formalism of CL dynamics and Lefschetz thimbles. Chapter 3 discusses the numerical setup of the CL simulations. In Chapter 4, we introduce a specific density modification to enforce a single-thimble dominance and examine its impact on CL convergence. Based on these modifications, we summarize the method of additive density modification and give an explicit formula for correcting the bias introduced by them. Finally, in Chapter 5, we give a summary of our results and outline the directions for future research.

Die approbierte gedruckte Originalversion dieser Diplomarbeit ist an der TU Wien Bibliothek verfügbar
The approved original version of this thesis is available in print at TU Wien Bibliothek.
TU Bibliothek Your knowledge hub WIEN

Chapter 2

Theoretical Background

2.1 Scalar Field Theory in Zero Dimensions

To investigate the convergence behavior of the CL method in a controlled and analytically tractable setting, we consider a toy model of scalar field theory. The model is defined in a single space-time point and the only degree of freedom is an internal real scalar, which we will denote by ϕ. Although this model lacks spatial or temporal structure and exhibits no notion of locality or correlation, it provides a non-trivial saddle-point structure and a genuine sign problem. Such zero-dimensional theories are not merely academic exercises. They also appear in effective models of quantum systems with a finite number of degrees of freedom, such as matrix models in string theory. For instance, the IKKT matrix model is a SUSY zero-dimensional theory with a complex fermion determinant and serves as a non-perturbative candidate for string theory [25, 26]. The scalar model admits a natural generalization to a theory with an internal $O(n)$ symmetry. In these so-called $O(n)$-vector models, the degree of freedom is promoted to a real-valued vector $\vec{\phi} \in \mathbb{R}^n$ and the action is constructed to be invariant under $O(n)$ rotations. In the context of the zero-dimensional scalar model, the partition function reduces to an ordinary integral over the internal degree of freedom ϕ, treated as the *field*

$$Z = \int_{-\infty}^{\infty} d\phi \, \exp(-S[\phi]) \, . \tag{2.1}$$

The action may be real or complex, depending on the context of the model. In this work, we focus on models with a quartic interaction term and the action reads

$$S = \frac{\sigma}{2}\phi^2 + \frac{\lambda}{4}\phi^4 \tag{2.2}$$

with real λ and complex σ. In the regime of $\sigma > 0$ an analytical result is known

$$Z = \sqrt{\frac{\sigma}{2\lambda}} \exp\left(\frac{\sigma^2}{8\lambda}\right) \int_0^{\infty} d\xi \, \cosh\left(\frac{\xi}{4}\right) \exp\left[-\frac{\sigma^2}{8\lambda}\cosh\xi\right] = \sqrt{\frac{\sigma}{2\lambda}} \exp\left(\frac{\sigma^2}{8\lambda}\right) K_{\frac{1}{4}}\left(\frac{\sigma^2}{8\lambda}\right) \tag{2.3}$$

with the modified Bessel function of the second kind K_ν [27].
Such a complex action gives rise to oscillatory integrands. This behavior can render direct numerical integration or naive Monte-Carlo sampling intractable because the computational effort scales exponentially; therefore, despite its simplicity, the model features a true sign problem due to its complex action [10, 26, 28]. For that reason, the model is sufficient to illustrate the sign problem and even allows for a complete analysis of the saddle point structure and the decomposition into Lefschetz thimbles.

The origin of the sign problem lies in the complex nature of the action $S[\phi]$. For $Im(\sigma) \neq 0$, the imaginary part introduces rapid oscillations. As a result, contributions from different regions of the integration domain interfere destructively, leading to a highly suppressed signal-to-noise

Die approbierte gedruckte Originalversion dieser Diplomarbeit ist an der TU Wien Bibliothek verfügbar
The approved original version of this thesis is available in print at TU Wien Bibliothek.
TU Bibliothek Your knowledge hub WIEN

ratio in naive sampling approaches. Despite lacking spatial or temporal structure, the model exhibits multiple saddle points, each contributing to the partition function along distinct steepest descent paths. Interference between these paths can lead to qualitative changes in the partition function. Even though there is no notion of temperature or extensive thermodynamic quantities in zero dimensions, nonanalytic behavior in the partition function can still occur as σ is varied. These transitions, often associated with Stokes phenomena, can be interpreted as analogs of quantum phase transitions [29]. In this work, we explore the model's behavior as σ varies in the complex plane, while keeping $\lambda > 0$ fixed to ensure convergence of the integral (2.1).

2.2 The Path Integral and the Sign Problem

In quantum field theory (QFT), expectation values of observables are computed using functional integration over field configurations [30], which gives rise to the name *path integral*. Using the convention of Euclidean signature, this takes the form

$$\langle \mathcal{O} \rangle = \frac{1}{Z} \int \mathcal{D}\phi \, \mathcal{O}[\phi] e^{-S[\phi]}, \quad Z = \int \mathcal{D}\phi \, [\phi] e^{-S[\phi]} \,. \tag{2.4}$$

In the case of real-valued actions $S[\phi]$, the integrand is positive semi-definite, and the density $\frac{\exp(-S[\phi])}{Z}$ can be interpreted as a probability weight, allowing naive Monte-Carlo methods to be applied. However, in many physical settings, the action becomes complex valued. Some prominent examples are finite-density QCD [6], real-time dynamics [1, 31] or theories with topological terms [4]. In the case of complex actions, the integrand becomes oscillatory, and the density cannot be interpreted as a probability density. Because importance sampling relies on the interpretation as a probability density, this hinders most Monte-Carlo methods. This fact is known as the **sign problem**. There are some techniques to tame the sign problem, we only want to list a few. For a comprehensive review, see [10].

One of the most straightforward methods goes by the name of *reweighting* [32]. In the presence of an imaginary part of the action, the density in the integral Eq. (2.4) is split into a magnitude and a phase. The phase part is then understood as being part of the observable considered. Expectation values are calculated via

$$\langle \mathcal{O} \rangle_\rho = \frac{1}{Z_\rho} \int \mathcal{D}\phi \, \left(\mathcal{O}[\phi] e^{-iS_I[\phi]} \right) e^{-S_R[\phi]} = \frac{Z_{|\rho|}}{Z_\rho} \frac{1}{Z_{|\rho|}} \int \mathcal{D}\phi \, \left(\mathcal{O}[\phi] e^{-iS_I[\phi]} \right) e^{-S_R[\phi]} \tag{2.5}$$

$$= \frac{\langle \mathcal{O} \rangle_{|\rho|}}{\langle e^{-iS_I[\phi]} \rangle_{|\rho|}} \,. \tag{2.6}$$

The regions of configuration space that dominate the full path integral may have negligible probability under the new sampling measure. This mismatch results in an exponentially suppressed average phase,

$$\langle e^{-iS_I[\phi]} \rangle_{|\rho|} \sim e^{-V\Delta f}, \tag{2.7}$$

where V is the system volume and Δf is a free energy difference between the target and sampling distributions. Consequently, the signal-to-noise ratio degrades exponentially, making this method impractical for systems in the thermodynamic limit $V \to \infty$. This critical issue in reweighting methods is known as the *overlap problem*.

Another method of overcoming the sign problem is the reformulation of the theory into the so-called *dual variables* [33]. These are discrete degrees of freedom that replace the original degrees of freedom. In certain cases, this mapping completely eliminates the complex action, resulting in real and positive weights suitable for importance sampling. The mapping to dual

Die approbierte gedruckte Originalversion dieser Diplomarbeit ist an der TU Wien Bibliothek verfügbar
The approved original version of this thesis is available in print at TU Wien Bibliothek.
TU Bibliothek Your knowledge hub WIEN

variables is exact and also respects the symmetries of the original theory. The new degrees of freedom typically admit a geometric interpretation, e.g., loops for bosonic theories. The representation in terms of dual variables is only known for a certain class of theories [34]. Dual variables can be efficiently sampled using the *worm algorithm* [35] , originally introduced for spin systems. It is based on temporarily violating a constraint (e.g., current conservation), propagating the defect through the lattice, and restoring the constraint upon closure of the 'worm'. The newly created configuration is accepted or rejected based on a Metropolis criterion.

The Lefschetz thimble method [15] offers a geometrically motivated solution to the sign problem. The key idea is to interpret the path integral not as an integral over real configurations, but rather over a deformed contour in a complexified field space. This deformation is done in such a way that the phase fluctuations, which are responsible for the sign problem, are tamed. This is achieved by decomposing the integration domain into a sum over curved manifolds called *thimbles*, each associated with a saddle point of the analytically continued action. Along these thimbles, the phase of the integrand remains constant, which reduces destructive interference between different field configurations. Instead of sampling from the entire oscillatory space of real configurations, one samples from the more stable, well-behaved region defined by the thimble. In practice, this method allows for a controlled evaluation of otherwise intractable integrals — provided the relevant thimbles and their contributions can be identified. While the method is mathematically elegant, it presents computational challenges, especially in higher dimensions where no efficient method of computing expansion coefficients (the so-called *intersection numbers*) is known to date [14].

2.3 The Complex Langevin Method and Its Convergence Problems

While techniques such as reweighting, dual variable formulations, and Lefschetz thimble decompositions offer insightful routes to mitigate the sign problem, they each come with their intrinsic limitations — from an exponentially growing number of samples needed in reweighting to practical challenges in computing intersection numbers for thimbles. This motivates the exploration of stochastic approaches that aim to circumvent these limitations without explicit contour deformation. One such method is the CL method, which extends the idea of stochastic quantization into the complexified field space. Despite its promise, CL is known to suffer from wrong convergence in many physically relevant scenarios. To understand these pathologies and the criteria under which CL can be trusted, we now turn to a study of its theoretical base and its potential failure. We begin with a review of Langevin dynamics in the real case and then extend the discussion to the complex domain.

2.3.1 The Case of Real Langevin

To build up towards the case of CL, we first consider the Langevin process for a real scalar ϕ and demonstrate that its stationary distribution $P(\phi)$ is unique under mild assumptions. This sets a baseline for understanding how and why the complex extension may fail. We follow the discussion in [36]. For the real scalar ϕ, we define the stochastic Langevin process parametrized by Langevin time τ

$$d\phi(\tau) = Kd\tau + d\omega(\tau) \tag{2.8}$$

Die approbierte gedruckte Originalversion dieser Diplomarbeit ist an der TU Wien Bibliothek verfügbar
The approved original version of this thesis is available in print at TU Wien Bibliothek.

where the drift is defined via $K = -\frac{\partial S}{\partial \phi(\tau)}$ and the Wiener process [37] satisfies

$$\langle d\omega(\tau) \rangle = 0\,, \tag{2.9}$$

$$\langle d\omega(\tau_1) d\omega(\tau_2) \rangle = \begin{cases} 2\,d\tau_1 & \tau_1 = \tau_2 \\ 0 & \tau_1 \neq \tau_2\ . \end{cases} \tag{2.10}$$

The stochastic process is associated with a probability density $P(\phi, \tau)$, which, from a frequentist perspective, can be interpreted as the relative frequency of the scalar degree of freedom taking the value ϕ at Langevin time τ. It can be shown that the Fokker-Planck equation

$$\frac{\partial P(\phi,\tau)}{\partial \tau} = \frac{\partial}{\partial \phi}\left(\frac{\partial}{\partial \phi} + \frac{\partial S}{\partial \phi}\right) P(\phi,\tau) =: \hat{\mathcal{L}}_{FP}^{T} P(\phi,\tau) \tag{2.11}$$

holds. A probability distribution $P^{\infty}(\phi)$ that describes the equilibrated system must be stationary in the sense that it is an eigenfunction of $\hat{\mathcal{L}}_{FP}^{T}$ with eigenvalue 0. It can be obtained by integrating Eq. (2.11)

$$\left(\frac{\partial}{\partial \phi} + \frac{\partial S}{\partial \phi}\right) P^{\infty}(\phi) = C \tag{2.12}$$

with an integration constant C, which is fixed by a normalization condition. It is solved by $P^{\infty}(\phi) = \mathcal{N} \exp(-S[\phi])$. This indeed gives a real probability distribution, as long as $S[\phi]$ is real valued. We want to give a quick hint on how nonstationary solutions can be obtained. A separation ansatz

$$P(\phi,\tau) = \rho(\phi) e^{-\lambda \tau} \tag{2.13}$$

yields the Langevin time-independent equation

$$\hat{\mathcal{L}}_{FP}^{T}\, \rho(\phi) = -\lambda \rho(\phi)\,. \tag{2.14}$$

We note that $\hat{\mathcal{L}}_{FP}^{T}$ is not a Hermitian operator. To simplify further calculations, we define the auxiliary quantity

$$Q(\phi,\tau) = P(\phi,\tau) e^{S/2}\,. \tag{2.15}$$

Plugging this into Eq. (2.11) gives

$$\frac{\partial Q(\phi,\tau)}{\partial \tau} = -\left[-\frac{\partial^2}{\partial \phi^2} - \frac{1}{2}\frac{\partial^2 S}{\partial \phi^2} + \frac{1}{4}\left(\frac{\partial S}{\partial \phi}\right)^2\right] Q(\phi,\tau) =: -\hat{H}_{FP}\, Q(\phi,\tau) \tag{2.16}$$

with the hermitian $\hat{H}_{FP}$ Fokker-Planck Hamiltonian operator [38]. In this Schrödinger-like equation, the probability density takes the form of a state vector in quantum mechanics and the Fokker-Planck Hamiltonian generates a translation in Langevin time. For every eigenfunction $\rho_n(\phi)$ of $\hat{\mathcal{L}}_{FP}$ with eigenvalue λ_n there exists an eigenfunction $\psi_n(\phi)$ of $-\hat{H}_{FP}$ with the same eigenvalue λ_n defined by

$$\psi_n(\phi) = e^{S/2} \rho_n(\phi)\,. \tag{2.17}$$

Die approbierte gedruckte Originalversion dieser Diplomarbeit ist an der TU Wien Bibliothek verfügbar
The approved original version of this thesis is available in print at TU Wien Bibliothek.
TU Bibliothek Your knowledge hub WIEN

It can be shown that for an appropriate choice of boundary conditions all eigenvalues λ_n are positive for $n > 1$ [38]. A full Langevin time-dependent solution is given in terms of a spectral decomposition

$$Q(\phi, \tau) = \sum_{n=0}^{\infty} a_n Q_n(\phi) e^{-\lambda_n \tau} . \tag{2.18}$$

The Fourier coefficients can be calculated based on an orthogonality argument about the eigenfunctions $Q_n(\phi)$. Especially the first coefficient a_0 turns out to be $1/\int d\phi \exp(-S)$. Here we used the fact that the probability is conserved at all Langevin times

$$\int d\phi P(\phi, \tau) = 1 . \tag{2.19}$$

All the other coefficients depend on the initial configuration of the system. We note that $Q_0(\phi) = \exp(-S(\phi)/2)$ is indeed an eigenfunction of $-\hat{H}_{FP}$ with eigenvalue $\lambda_0 = 0$. Therefore we recover the stationary solution in Q as

$$\lim_{\tau \to \infty} Q(\tau, \phi) = a_0 Q_0(\phi) = \frac{\exp(-S(\phi)/2)}{\int d\phi \, \exp(-S(\phi))} . \tag{2.20}$$

In terms of the probability distribution P this gives

$$\lim_{\tau \to \infty} P(\tau, \phi) = \frac{\exp(-S(\phi))}{\int d\phi \, \exp(-S(\phi))} = P^{\infty}(\phi) . \tag{2.21}$$

This statement is independent of the initial configuration of the system and we can define observable averages as the limiting process

$$\langle \mathcal{O}[\phi] \rangle = \lim_{\tau \to \infty} \langle \mathcal{O}[\phi(\tau)] \rangle . \tag{2.22}$$

A crucial aspect of implementing a Langevin-like algorithm is that ergodicity ensures the following relationship:

$$\langle \mathcal{O}[\phi] \rangle = \lim_{T \to \infty} \frac{1}{T} \int_{T_0}^{T_0 + T} d\tau \, \mathcal{O}[\phi(\tau)] . \tag{2.23}$$

with the so-called thermalization time T_0. This means that observable averages can be computed as path/ensemble averages over Langevin time. If a stationary probability distribution exists, it is unique and we can be certain that the averaging along Langevin time gives correct results. These observations form the basis of the stochastic quantization technique [16]. Fig. 2.1 shows how a real Langevin simulation reproduces $P(\phi, \tau \to \infty)$. This was done for $\sigma = \pm 1$ and $\lambda = 2$.

2.3.2 The Case of Complex Langevin

In its core, the CL method generalizes the idea of stochastic quantization [16] and allows the action to take on complex values. For theories with a complex-valued action S, the degrees of freedom ϕ defined on a manifold $\mathcal{M}$ are analytically continued to $\phi_c = \phi_R + i\phi_I$ in a complexified field space $\mathcal{M}_c$. The action S and all observables $\mathcal{O}$ are assumed to be holomorphic functions of ϕ_c. The CL equation then defines the evolution of ϕ_c in $\mathcal{M}_c$ with respect to Langevin time and

Die approbierte gedruckte Originalversion dieser Diplomarbeit ist an der TU Wien Bibliothek verfügbar
The approved original version of this thesis is available in print at TU Wien Bibliothek.
TU Bibliothek Your knowledge hub WIEN

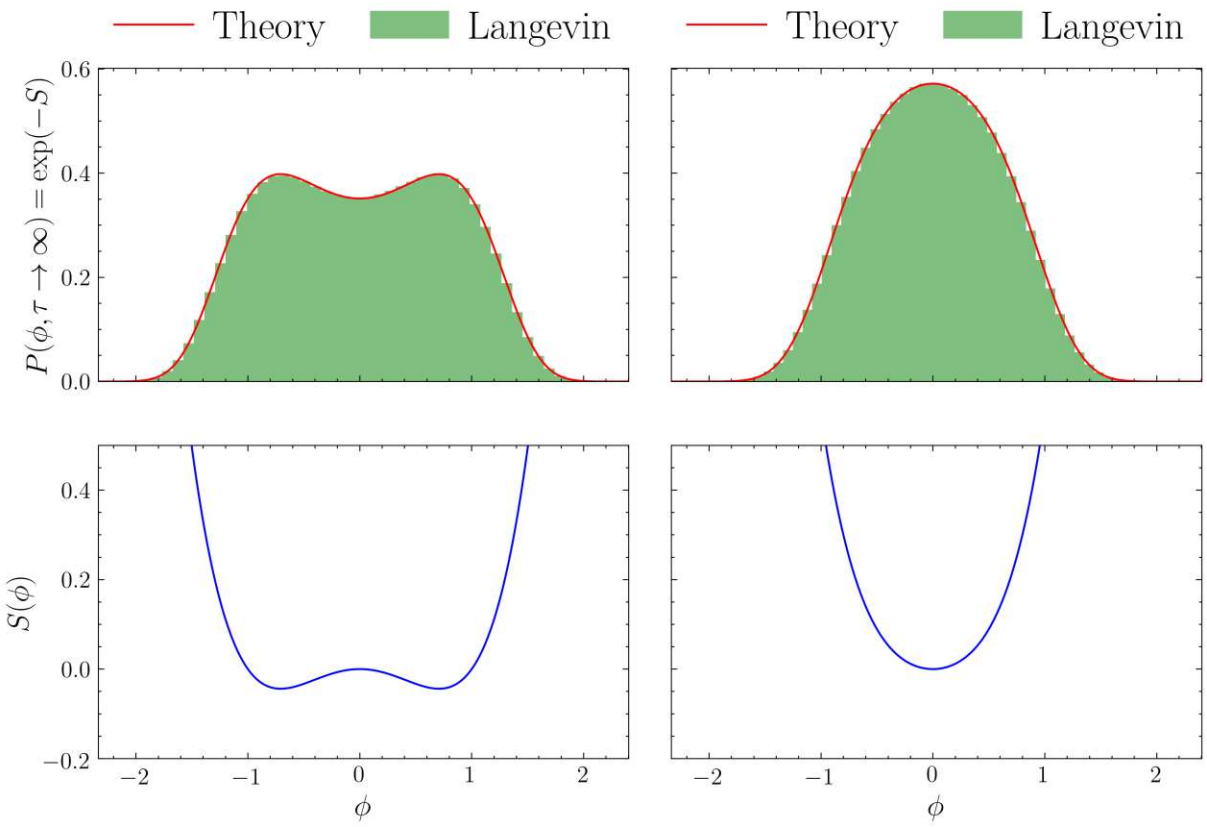

Fig. 2.1: The histogram of the real Langevin method reproduces the reproduces $P(\phi, \tau \to \infty)$ in both the case of $\mathrm{Re}(\sigma) > 0$ and $\mathrm{Re}(\sigma) < 0$. Here $\sigma = +1$ (left upper), $\sigma = -1$ (right upper) and $\lambda = 2$ were chosen. The lower panel shows the corresponding action $S(\phi) = \frac{\sigma}{2}\phi^2 + \frac{\lambda}{4}\phi^4$

it is characterized by a real probability density $P(\phi_c)$ over $\mathcal{M}_c$. The dynamics are determined by the complex analog of (2.8):

$$d\phi_R = \mathrm{Re}(K)\, d\tau + d\omega_R(\tau)\,, \tag{2.24}$$

$$d\phi_I = \mathrm{Im}(K)\, d\tau + d\omega_I(\tau)\,. \tag{2.25}$$

$\omega(\tau)_{R/I}$ is again the Wiener process that satisfies (2.10). Without loss of generality, we choose $d\omega_I(\tau) = 0$ [39]. Observables in the complexified field space are calculated via

$$\langle \mathcal{O} \rangle_{\mathcal{M}_c} = \frac{1}{\int_{\mathcal{M}_c} d\phi_c\, P(\phi_c)} \int_{\mathcal{M}_c} d\phi_c\, \mathcal{O}(\phi_c) P(\phi_c)\,. \tag{2.26}$$

The CL method can be considered successful if and only if its results agree with observables

$$\langle \mathcal{O} \rangle_{\mathcal{M}} = \frac{1}{\int_{\mathcal{M}} d\phi\, \rho(\phi)} \int_{\mathcal{M}} d\phi\, \mathcal{O}(\phi)\rho(\phi) \quad \text{with } \rho(\phi) = e^{-S[\phi]} \tag{2.27}$$

computed in the original field space on basis of the complex density $\rho(\phi)$. If so, the sign problem may be avoided, as $P(\phi_c)$ can be inferred from histograms of the CL process [10, 40]. Unfortunately, examples are known to violate this equality [17]. This issue was discussed in

Die approbierte gedruckte Originalversion dieser Diplomarbeit ist an der TU Wien Bibliothek verfügbar
The approved original version of this thesis is available in print at TU Wien Bibliothek.

[9, 17] and conditions of the correctness of this approach were developed. We want to summarize the main features of the formal justification of the CL method.

For the following discussion we define the Langevin time dependent *expectation values* as

$$\langle \mathcal{O} \rangle_{P(\tau)} = \langle \mathcal{O} \rangle_{\mathcal{M}_c} [P \to P(\tau)] \,, \tag{2.28}$$

$$\langle \mathcal{O} \rangle_{\rho(\tau)} = \langle \mathcal{O} \rangle_{\mathcal{M}} [\rho \to \rho(\tau)] \,. \tag{2.29}$$

The real probability distribution $P(\phi_c, \tau)$ over $\mathcal{M}_c$ and the complex probability distribution $\rho(\phi, \tau)$ over $\mathcal{M}$ are generated by their corresponding real and complex Fokker-Planck equations

$$\frac{\partial}{\partial \tau} P(\phi_c, \tau) = \hat{\mathcal{L}}_{FP}^T P(\phi_c, \tau) \qquad \frac{\partial}{\partial \tau} \rho(\phi, \tau) = \hat{\mathcal{L}}_0^T \rho(\phi, \tau) \tag{2.30}$$

with the real Fokker-Planck operator

$$\hat{\mathcal{L}}_{FP}^T = \partial_{\phi_R} (\partial_{\phi_R} + \mathrm{Re}\,[\partial_{\phi_c} S]) + \partial_{\phi_I} \mathrm{Im}[\partial_{\phi_c} S] \tag{2.31}$$

and the complex Fokker-Planck operator

$$\hat{\mathcal{L}}_0^T = \partial_{\phi_c} (\partial_{\phi_c} + \partial_{\phi_c} S) \,. \tag{2.32}$$

CL will give the correct results if the correspondence

$$\langle \mathcal{O} \rangle_{P(0)} = \langle \mathcal{O} \rangle_{\rho(0)} \tag{2.33}$$

remains valid for all later Langevin times

$$\langle \mathcal{O} \rangle_{P(\tau)} = \langle \mathcal{O} \rangle_{\rho(\tau)} \,. \tag{2.34}$$

To show this, we consider the Langevin time evolution of holomorphic observables. According to Ito calculus, the equation

$$\partial_\tau \mathcal{O}(\phi_c, \tau) = \hat{\mathcal{L}}_{FP}\, \mathcal{O}(\phi_c, \tau) \tag{2.35}$$

holds with the transposed Fokker-Planck operator

$$\hat{\mathcal{L}}_{FP} = \partial_{\phi_R} (\partial_{\phi_R} - \mathrm{Re}\,[\partial_{\phi_c} S]) - \partial_{\phi_I} \mathrm{Im}[\partial_{\phi_c} S] \,. \tag{2.36}$$

It generates the semigroup $\exp(t\hat{\mathcal{L}}_{FP})$. The central object concerning the criterion of correctness is the interpolator

$$F(t, \tau) := \int_{\mathcal{M}_c} d\phi_c \, P(\phi_c, t - \tau)\, \mathcal{O}(\phi_c, \tau) \quad \tau \in [0, t] \,. \tag{2.37}$$

It has the property $F(t, 0) = \langle \mathcal{O} \rangle_{P(t)}$ and $F(t, t) = \langle \mathcal{O} \rangle_{\rho(t)}$, which can be seen by choosing initial conditions (without loss of generality) $P(\phi_c, 0) = \rho(\phi, 0)\delta(\phi_I - a)$ for any $a \in \mathcal{M}$. We may choose such initial conditions, because in the limit of $\lim_{\tau \to \infty}$ ergodicity ensures that dependence on the initial conditions disappears. Using Eq. (2.30) and Eq. (2.35) the derivative of $F(t, \tau)$ reads

$$\frac{\partial F(t, \tau)}{\partial \tau} = - \int_{\mathcal{M}_c} d\phi_c \, \hat{\mathcal{L}}_{FP}^T P(\phi_c, t - \tau)\, \mathcal{O}(\phi_c, \tau) + \int_{\mathcal{M}_c} d\phi_c \, P(\phi_c, t - \tau)\, \hat{\mathcal{L}}_{FP} \mathcal{O}(\phi_c, \tau) \,. \tag{2.38}$$

Die approbierte gedruckte Originalversion dieser Diplomarbeit ist an der TU Wien Bibliothek verfügbar
The approved original version of this thesis is available in print at TU Wien Bibliothek.
TU Bibliothek Your knowledge hub WIEN

These two terms cancel if the boundary terms introduced by partial integration vanish. If this is the case $F(t,\tau)$ is constant in τ. This would imply that indeed $\langle\mathcal{O}\rangle_{P(\tau)} = \langle\mathcal{O}\rangle_{\rho(\tau)}$. Therefore, the criterion of correctness is formulated in terms of the asymptotic behavior of combinations of the probability distribution $P(\phi_c,\tau)$ and observables $\mathcal{O}(\phi_c,\tau)$ towards large amplitudes of ϕ_c. However, while this criterion is sufficient, it is considered *academic* [17] in the sense that one would have to check the asymptotic behavior for infinitely many base observables. These could, for example, be modes e^{ikx} for all $k \in \mathbb{Z}$. Additionally, the criterion is checked after a simulation is performed, which further reduces its applicability. Despite these limitations, the criterion has been successfully applied in many instances, see, for example, [3, 41–44]. The criterion may be violated whenever $\mathcal{M}_c$ forms a non-compact manifold. This can be the case for originally compact examples like $SU(N)$ symmetric theories, which are complexified to non-compact $SL(N,\mathbb{C})$ groups. There, a gauge cooling procedure can be used to ensure that the criterion of correctness is fulfilled [45].

Another independent factor can hinder the proper convergence of the CL method. If one allows a meromorphic drift $\partial_\phi S$, that is, holomorphic on $\mathcal{M}_c$ except for a set of isolated points (poles), the probability density must be suppressed in the vicinity of these poles. This was proposed in [46] and further discussed in [47, 48]. Given its relevance in a subsequent chapter, we now reflect on the key insights from [47]. The derivation of this criterion differs from the criterion based on the probability distribution in $\mathcal{M}_c$ in the sense that the authors consider a finite Langevin time step ϵ.
We want to show that

$$\lim_{\epsilon\to 0}\lim_{\tau\to\infty}\langle\mathcal{O}\rangle_{P(\tau)} = \langle\mathcal{O}\rangle_{\mathcal{M}}\,, \tag{2.39}$$

with $\langle\mathcal{O}\rangle_{\mathcal{M}}$ according to Eq. (2.27). We consider the Langevin time-evolved quantity

$$\langle\mathcal{O}\rangle_{P(\tau+\epsilon)} = \int_{\mathcal{M}_c} d\phi_c\, P(\phi_c,\tau+\epsilon)\mathcal{O}(\phi_c)\,. \tag{2.40}$$

If the left hand side of Eq. (2.39) exists, the time evolved expectation value can be written as [47]

$$\langle\mathcal{O}\rangle_{P(\tau+\epsilon)} \propto \int_{\mathcal{M}_c} d\phi_c\, P(\phi_c,\tau)\mathcal{O}_\epsilon(\phi_c) \tag{2.41}$$

with

$$\mathcal{O}_\epsilon(\phi_c) \propto \int d\eta\, e^{-\frac{1}{4}\eta^2}\mathcal{O}\left(\phi_c - \epsilon\partial_\phi S + \sqrt{\epsilon}\eta\right)\,. \tag{2.42}$$

Next, we expand $\mathcal{O}_\epsilon(\phi_c)$ in epsilon and find

$$\mathcal{O}_\epsilon(\phi_c) \propto \int d\eta\, e^{-\frac{1}{4}\eta^2}\left[\mathcal{O}(\phi_c) + \sum_{n=1}^{\infty}\frac{\sqrt{\epsilon^n}}{n!}\frac{\partial^n\mathcal{O}}{\partial\phi_c^n}\eta^n + \sum_{n=1}^{\infty}\frac{\epsilon^n}{n!}\frac{\partial^n\mathcal{O}}{\partial\phi_c^n}\left(-\frac{\partial S}{\partial\phi_c}\right)^n\right]\,. \tag{2.43}$$

Using standard Gaussian integrals, we can integrate out η and get

$$\mathcal{O}_\epsilon(\phi_c) \propto \sqrt{4\pi}\left(\mathcal{O}(\phi_c) + \sum_{n=1}^{\infty}\frac{\epsilon^n}{(2n)!}\frac{\partial^{2n}\mathcal{O}}{\partial\phi_c^{2n}}(2n-1)!!2^n + \sum_{n=1}^{\infty}\frac{\epsilon^n}{n!}\frac{\partial^n\mathcal{O}}{\partial\phi_c^n}\left(-\frac{\partial S}{\partial\phi_c}\right)^n\right)\,. \tag{2.44}$$

Die approbierte gedruckte Originalversion dieser Diplomarbeit ist an der TU Wien Bibliothek verfügbar
The approved original version of this thesis is available in print at TU Wien Bibliothek.
TU Bibliothek Your knowledge hub WIEN

The known formula for double factorials gives the simple formula

$$\mathcal{O}_\epsilon(\phi_c) \propto \mathcal{O}(\phi_c) + \sum_{n=1}^{\infty} \frac{\epsilon^n}{n!} \left[\left(-\frac{\partial S}{\partial \phi_c} \right)^n + \frac{\partial^n}{\partial \phi_c^n} \right] \frac{\partial^n}{\partial \phi_c^n} \mathcal{O}(\phi_c) \tag{2.45}$$

Plugging this back in Eq. (2.41) gives

$$\langle \mathcal{O} \rangle_{P(\tau+\epsilon)} \propto \int_{\mathcal{M}_c} d\phi_c \, P(\phi_c, \tau) \left[\mathcal{O}(\phi_c) + \sum_{n=1}^{\infty} \frac{\epsilon^n}{n!} \left[\left(-\frac{\partial S}{\partial \phi_c} \right)^n + \frac{\partial^n}{\partial \phi_c^n} \right] \frac{\partial^n}{\partial \phi_c^n} \mathcal{O}(\phi_c) \right] \tag{2.46}$$

$$= \langle \mathcal{O} \rangle_{P(\tau)} + \epsilon \int_{\mathcal{M}_c} d\phi_c \, P(\phi_c, \tau) \left[\hat{\mathcal{L}}_{FP} \mathcal{O}(\phi_c) \right] + O(\epsilon^2) \tag{2.47}$$

with the Fokker-Planck operator as defined in Eq. (2.36). This formula can be used to extract the Langevin time derivative of $P(\phi_c, \tau)$

$$\frac{\partial \langle \mathcal{O} \rangle_{P(\tau)}}{d\tau} := \lim_{\epsilon \to 0} \frac{\langle \mathcal{O} \rangle_{P(\tau+\epsilon)} - \langle \mathcal{O} \rangle_{P(\tau)}}{\epsilon} = \int_{\mathcal{M}_c} d\phi_c \, P(\phi_c, \tau) \left[\hat{\mathcal{L}}_{FP} \mathcal{O}(\phi_c) \right] . \tag{2.48}$$

This is nothing but the partially integrated Fokker-Plank equation modulo boundary terms. However, as discussed above, these boundary terms do not necessarily vanish. The authors in [47] argue that this conundrum should be attributed to a vanishing convergence radius of (2.46); these integrals may fail to converge for arbitrary powers of n. Moreover, even if they do converge at a given Langevin time τ_0, the radius of convergence may not be uniformly bounded for all later Langevin times.

The criterion of correctness is therefore a statement about the behavior of the dominating term in (2.46) which for large n is

$$Q^{(n)} = \int_{\mathcal{M}_c} d\phi_c \, P(\phi_c, \tau) \left(-\frac{\partial S}{\partial \phi_c} \right)^n . \tag{2.49}$$

We may rewrite it in terms of a distribution of drift magnitudes

$$Q^{(n)} = \int_0^\infty du \, u^n p(u) \qquad p(u) = \int_{\mathcal{M}_c} d\phi_c \, \delta \left(\left| \frac{\partial S}{\partial \phi_c} \right| + u \right) P(\phi_c, \tau) . \tag{2.50}$$

If Eq. (2.46) exists, $p(u)$ must be stronger suppressed than any power of u for large u. We interpret $p(u)$ as a *drift histogram*: it measures the distribution of drift magnitudes encountered by the process on the complexified manifold. This shows that the validity of the CL method depends crucially on the suppression of large drift regions, which may be violated if the process samples near poles or fails to decay at infinity. The criterion based on the drift histogram is considered sufficient and necessary for the correctness of the CL method, for further discussion, see [46, 48–50].

2.4 Lefschetz Thimble Decomposition

The challenges faced by the CL method, particularly its wrong convergence behavior in certain regimes, may not be arbitrary pathologies but rather are expected to reflect the intricate structure of the underlying path integral. A deeper understanding of these failures may emerge from the geometry of the complexified field space [20, 51]. Specifically, the formalism of Lefschetz thimbles provides a powerful framework for analyzing which regions in field space contribute meaningfully to the path integral, and how phase cancellations shape the result. Each thimble is associated with

Die approbierte gedruckte Originalversion dieser Diplomarbeit ist an der TU Wien Bibliothek verfügbar
The approved original version of this thesis is available in print at TU Wien Bibliothek.
TU Bibliothek Your knowledge hub WIEN

a critical point of the analytically continued action and integration along these steepest descent contours ensures maximal suppression of phase fluctuations. This geometric decomposition thus serves as both a diagnostic and a potential remedy for CL convergence issues. In the following, we introduce the mathematical foundation of the Lefschetz thimble decomposition, based on a physically motivated presentation rather than a rigorous mathematical treatment. For formal proofs and a more complete mathematical framework, we refer to [14, 51, 52]. We begin by considering integrals of the form

$$Z = \int_{-\infty}^{\infty} d\phi \, e^{-S(\phi)}, \tag{2.51}$$

where $S : \mathbb{C} \to \mathbb{C}$ is a holomorphic or meromorphic function representing the complexified action. In the *unmodified* case, the action S and the drift $\partial S/\partial \phi_c$ are holomorphic functions in $\mathbb{C}$ (polynomials). In the *modified* case we allow the drift to be meromorphic in $\mathbb{C}$, that is, holomorphic in $\mathbb{C}\backslash P$ where P is a set of isolated poles of $\partial S/\partial \phi$.

To start the discussion on Lefschetz thimbles, consider the integral

$$Z_{\Gamma^{(ij)}} = \int_{\Gamma^{(ij)}} d\phi_c \, e^{-S(\phi_c)} \tag{2.52}$$

where $\Gamma^{(ij)}$ is a contour in $\mathbb{C}$ connecting two regions Ω_i and Ω_j at infinity, or possibly forming a non-contractible loop. The non-contractible loop is only relevant in the modified case, where singularities of the integrand are present. We require that

$$\mathrm{Re}S(\phi_c) \to +\infty \qquad \text{for } |\phi_c| \to \infty, \ \phi_c \in \Omega_i \cup \Omega_j, \tag{2.53}$$

to ensure convergence of the integral. If Eq. (2.52) exists, we refer to $\Gamma^{(ij)}$ as an *integration cycle*, following the terminology of Refs. [14, 51]. The identity

$$\int_{\Gamma^{(ij)}} d\phi_c \ + \int_{\Gamma^{(jk)}} d\phi_c = \int_{\Gamma^{(ik)}} d\phi_c \tag{2.54}$$

holds. It follows that $\Gamma^{ij} = -\Gamma^{ji}$, which in the integral sense means nothing more than a change of orientation. Without loss of generality, we fix an orientation and label the cycles Γ^{ij} by γ_i. The cycles γ_i will be chosen such that they form a basis of the first relative homology group $H_1(\mathbb{C}, (\mathbb{C})^T; \mathbb{Z})$ for large T where $(\mathbb{C})^T = \{z \in \mathbb{C} \mid Re[S(z)] > T\}$ are regions in which the action decreases rapidly [14, 52]. The original integration contour (the real line) is itself an element of this homology group and can therefore be decomposed into a linear combination of these basis cycles.

In Refs. [9, 26] a connection between the correct convergence of CL and the Dyson-Schwinger Equations (DSE) was established. It is assumed, that absence of boundary terms in a complex Langevin simulation imply the Dyson–Schwinger equations [53]. Further, in [54] it was proven that any linear functional on a suitable space of test functions satisfying the SDE can be represented as a linear combination of integrals along curves γ_i. Consequently, if boundary terms vanish, observables calculated by CL take the form [53]

$$\langle \mathcal{O} \rangle_{CL} = \sum_{i=1}^{N_\gamma} a_i \frac{\int_{\gamma_i} d\phi_c \, \mathcal{O}(\phi_c) \exp(-S[\phi_c])}{\int_{\gamma_i} d\phi_c \, \exp(-S[\phi_c])} \, . \tag{2.55}$$

A suitable choice of γ_i are so-called Lefschetz thimbles. To construct them, we assume that $Re(S[\phi_c])$ has non-degenerate critical points α. This classifies S as a *Morse* function. Applied to

Die approbierte gedruckte Originalversion dieser Diplomarbeit ist an der TU Wien Bibliothek verfügbar
The approved original version of this thesis is available in print at TU Wien Bibliothek.
TU Bibliothek Your knowledge hub WIEN

our case of a scalar Morse function $Re(S)$ from $\mathbb{C}$ to $\mathbb{R}$, the Morse theorem [55] guaranties that for every critical point α, there exists a local chart (ϕ_1, ϕ_2) in the neighborhood of α such that

$$Re(S[\phi]) = Re(S[\alpha]) - \phi_1^2 + \phi_2^2 \,. \tag{2.56}$$

Each critical point α defines a *downward flow equation*

$$\frac{d\phi_\alpha^*}{dt} = -\overline{\frac{\partial S}{\partial \phi}}\bigg|_{\phi_\alpha^*(t)} \qquad t \in \mathbb{R} \,. \tag{2.57}$$

The criticality of α makes it a fixed point of the flow equation. Using this, we define the Lefschetz thimble $\mathcal{J}_\alpha$ as the union of all flows that satisfy the flow equation and therefore the fixed point condition

$$\mathcal{J}_\alpha = \{\phi(t) \in \mathbb{C} \mid \phi(t \to \infty) = \alpha\}, \quad \phi(t) \text{ solves Eq. (2.57)} \,. \tag{2.58}$$

We note two key properties of the Lefschetz thimble that follow directly from Eq. (2.57). First, the real part of the action is monotonic along the thimble. Second, the imaginary part of S is constant along the thimble. Both these statements follow from the insight that the change of S with t reads

$$\frac{dS}{dt} = \frac{\partial S}{\partial \phi}\frac{d\phi}{dt} = -\left|\frac{\partial S}{\partial \phi}\right|^2 < 0 \in \mathbb{R} \,. \tag{2.59}$$

It is real-valued and decreases with flow time t. Since the change is real valued, the imaginary part of S must be constant along individual thimbles $\mathcal{J}_\alpha \, \forall \alpha$. Further, for $t \to \infty$, the real part of the action tends towards $+\infty$. We call this limit the *end* of the thimble. This feature guarantees that the integrand $\exp(-S)$ tends to zero and the *end* of the thimble. Due to the monotonic behavior of $\mathrm{Re}(S)$ along the thimble (see Eq. (2.59)), the flow can only terminate at another critical point, a singularity (if present), or at infinity. These are the only allowed endpoints of a Lefschetz thimble. The statement about the asymptotic behavior makes $\mathcal{J}_\alpha$ an element of the relative homology $H_1(\mathbb{C}, (\mathbb{C})^T; \mathbb{Z})$. Indeed, $\mathcal{J}_\alpha$ form a basis of $H_1(\mathbb{C}, (\mathbb{C})^T; \mathbb{Z})$. This means that if $\mathcal{D}$ lies in the relative homology, there exists a decomposition using the Lefschetz thimble basis [14, 51]

$$\int_{\mathcal{D}} d\phi \, e^{-S(\phi)} = \int_{\sum_\alpha n_\alpha \mathcal{J}_\alpha} d\phi_c \, e^{-S(\phi_c)} = \sum_\alpha n_\alpha e^{-Im[S(\phi_c)]} \int_{\mathcal{J}_\alpha} d\phi_c \, e^{-Re[S(\phi_c)]} \,. \tag{2.60}$$

The coefficients n_α are given by the number of intersections of the dual thimble $\mathcal{K}_\alpha$ with the original domain of integration $\mathcal{D}$, as shown by *Witten* in [14, 51]. The dual thimble $\mathcal{K}_\alpha$ is the union of all flows that satisfy the upward flow equation

$$\frac{d\phi_\alpha^*}{dt} = +\overline{\frac{\partial S}{\partial \phi}}\bigg|_{\phi_\alpha^*(t)} \tag{2.61}$$

$$\mathcal{K}_\alpha = \{\phi(t) \in \mathbb{C} \mid \phi(t \to \infty) = \alpha\}, \quad \phi(t) \text{ solves Eq. (2.61)} \,. \tag{2.62}$$

We refer to thimbles with coefficients $n_\alpha \neq 0$ as relevant. Using a similar argument, the imaginary part of S is also constant along $\mathcal{K}_\alpha$. The real part of S tends towards $-\infty$ at the *end* of the dual thimble. Importantly, this result is structurally the same as the prescription Eq. (2.55). It has been observed that the dynamics of the CL method are intimately connected to the underlying

Die approbierte gedruckte Originalversion dieser Diplomarbeit ist an der TU Wien Bibliothek verfügbar
The approved original version of this thesis is available in print at TU Wien Bibliothek.
TU Bibliothek Your knowledge hub WIEN

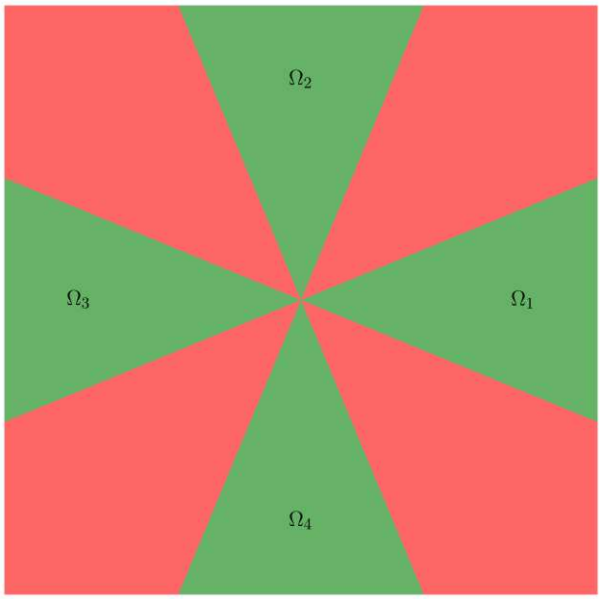

Fig. 2.2: The integral Z_Γ can only be defined for integration paths Γ that connect certain regions Ω at infinity. It is necessary for the integrand to vanish far out in these regions. The green sections Ω_{1-4} represent regions that fulfill this property.

Lefschetz thimble structure of the theory [18–21]. It was even conjectured that CL gives correct results, if there is a single relevant thimble associated with a attractive critical point. This would imply that CL can be understood as importance sampling on a single relevant Lefschetz thimble. If multiple thimbles are relevant, the imaginary parts in Eq. (2.55) do not cancel but rather interfere. In later sections, we show how CL convergence can be restored by modifying the underlying Lefschetz thimble structure of the theory. First, we study the Lefschetz thimble structure of the unmodified and the modified theory.

2.4.1 Unmodified Theory

In this section, we study the Lefschetz thimble structure of the anharmonic oscillator with a complex mass parameter σ. The action is given by $S = \frac{\sigma}{2}\phi^2 + \frac{\lambda}{4}\phi^4$, and we choose the polar parametrization $\phi = \rho e^{i\theta}$, $\sigma = \sigma_r e^{i\sigma_\phi}$. For completeness, we also allow a complex self-interaction term $\lambda = \lambda_r e^{i\lambda_\phi}$, which we later restrict to real coupling ($\lambda_\phi = 0$).

We isolate the real part of $S(\rho, \theta)$ and get

$$\mathrm{Re}S(\rho,\theta) = \frac{\sigma_r}{2}\rho^2\cos(\sigma_\phi + 2\theta) + \frac{\lambda_r}{4}\rho^4\cos(\lambda_\phi + 4\theta)\,. \tag{2.63}$$

From this, we observe that $\mathrm{Re}S(z)$ behaves like $\frac{\lambda_r}{4}\rho^4\cos(\lambda_\phi + 4\theta)$ for $\rho \to \infty$ and Eq. (2.53) implies that $\cos(\lambda_\phi + 4\theta) > 0$ or

$$\theta \in \bigcup_{n\in\mathbb{Z}} \left(\frac{2n\pi - \lambda_\phi}{4}, \frac{2n\pi + \pi - \lambda_\phi}{4} \right)\,. \tag{2.64}$$

As an example, consider real coupling $\lambda_\phi = 0$. This yields four sectors of width $\frac{\pi}{2}$, centered along directions $\theta = \frac{k\pi}{2}$ for $k \in \{0, 1, 2, 3\}$; see Figure 2.2 for a schematic illustration. Generic coupling rotates the four sectors by λ_θ. Lefschetz thimbles are valid choices for integration

Die approbierte gedruckte Originalversion dieser Diplomarbeit ist an der TU Wien Bibliothek verfügbar
The approved original version of this thesis is available in print at TU Wien Bibliothek.
TU Bibliothek Your knowledge hub WIEN

contours Γ because Equation (2.53) is automatically satisfied due to the monotonicity of Re(S) along the flow. The thimbles and their corresponding duals are defined via the downward and upward flow equations and their respective critical point:

$$\frac{d\phi_\gamma(t)}{dt} = \mp\overline{\frac{\partial S}{\partial \phi}}\Big|_{\phi_\alpha(t)} \qquad \lim_{t\to\infty}\phi_\alpha(t) = \alpha\,. \tag{2.65}$$

where the thimble takes the upper $(-)$ and the dual thimble the lower sign $(+)$. In our representation, the flow equation reads under the use of the product rule of differentiation

$$\mp(\partial_t\rho + i\rho\partial_t\theta)e^{i\theta} = \sigma_r e^{-i(\sigma_\phi+\theta)}\rho + \lambda_r e^{-i(\lambda_\phi+3\theta)}\rho^3\,. \tag{2.66}$$

Dividing this by $\phi = \rho e^{i\theta}$ gives

$$\mp(\partial_t\log(\rho) + i\partial_t\theta) = \sigma_r e^{-i(\sigma_\phi+2\theta)} + \lambda_r e^{-i(\lambda_\phi+4\theta)}\rho^2\,. \tag{2.67}$$

We can split this expression into real and imaginary parts and compare those

$$\text{Real:}\quad \mp\,\partial_t\log\rho = \sigma_r\cos(\sigma_\phi+2\theta) + \lambda_r\rho^2\cos(\lambda_\phi+4\theta)\,, \tag{2.68}$$

$$\text{Imaginary:}\quad \pm\,\partial_t\theta = \sigma_r\sin(\sigma_\phi+2\theta) + \lambda_r\rho^2\sin(\lambda_\phi+4\theta)\,. \tag{2.69}$$

At this point, the equation is exact and valid at all flow times t. Let us assume that in the limit $\lim_{t\to-\infty}\theta$ converges to a constant θ^0. This manifests itself as a thimble, which extends towards a definite direction in the complex plane. In the larger negative t limit, this takes the form $\partial_t\theta = 0$ and the equation for the imaginary part reads

$$0 = \sigma_r\sin(\sigma_\phi+2\theta^0) + \lambda_r\sin(\lambda_\phi+4\theta^0)\rho^2\,. \tag{2.70}$$

Because $\rho\in\mathbb{R}$ per definition, we obtain the condition:

$$\rho^2 = -\frac{\sigma_r}{\lambda_r}\frac{\sin(\sigma_\phi+2\theta)}{\sin(\lambda_\phi+4\theta)} > 0\,. \tag{2.71}$$

The assumption $\partial_t\theta = 0$ therefore gives allowed sectors in which thimbles can extend

$$\sin(\sigma_\phi+2\theta^0) > 0 : \theta^0 \in \bigcup_{n\in\mathbb{Z}}\left(\frac{\pi\cdot 2n-\sigma_\phi}{2}, \frac{\pi\cdot(2n+1)-\sigma_\phi}{2}\right), \tag{2.72}$$

$$\sin(\lambda_\phi+4\theta^0) < 0 : \theta^0 \in \bigcup_{n\in\mathbb{Z}}\left(\frac{\pi\cdot(2n-1)-\lambda_\phi}{4}, \frac{\pi\cdot 2n-\lambda_\phi}{4}\right), \tag{2.73}$$

$$\text{or} \tag{2.74}$$

$$\sin(\lambda_\phi+2\theta^0) < 0 : \theta^0 \in \bigcup_{n\in\mathbb{Z}}\left(\frac{\pi\cdot(2n-1)-\lambda_\phi}{4}, \frac{\pi\cdot 2n-\lambda_\phi}{4}\right), \tag{2.75}$$

$$\sin(\lambda_\phi+4\theta^0) > 0 : \theta^0 \in \bigcup_{n\in\mathbb{Z}}\left(\frac{\pi\cdot 2n-\lambda_\phi}{4}, \frac{\pi\cdot(2n+1)-\lambda_\phi}{4}\right). \tag{2.76}$$

Die approbierte gedruckte Originalversion dieser Diplomarbeit ist an der TU Wien Bibliothek verfügbar
The approved original version of this thesis is available in print at TU Wien Bibliothek.
TU Bibliothek Your knowledge hub WIEN

We can refine these sectors using the following observation in Eq. (2.71): Thimbles that extend to infinity in a direction θ^0 demand the expression for ρ^2 to diverge for certain θ^0. Algebraically, this happens if $\sin(\lambda_\phi + 4\theta^0) = 0 \neq \sin(\sigma_\phi + 2\theta^0)$ which defines directions

$$\theta^0 = \frac{n\pi - \lambda_\phi}{4} \neq \frac{m\pi - \sigma_\phi}{2} \qquad \text{for } (n, m) \in \mathbb{Z}\,. \tag{2.77}$$

Therefore, thimbles that connect a critical point with infinity can only do so in certain directions. In the case of real coupling, these are the real and the imaginary axes as well as the diagonals in the four quadrants of the complex plane.

Thimbles that connect a critical point with another critical point or a singularity must necessarily meet $\partial_t \theta = 0$ in the large negative flow time limit. We can again use Eq. (2.71) and require $\rho \to \rho_0 < \infty$. This forces $\sin(\sigma_\phi + 2\theta) = \sin(\lambda_\phi + 4\theta)$ which defines directions

$$\theta^0 = \frac{n\pi - \lambda_\phi}{4} = \frac{m\pi - \sigma_\phi}{2} \qquad \text{for } (n, m) \in \mathbb{Z}\,. \tag{2.78}$$

These statements hold for both thimbles and their duals. In the case of extended thimbles, one can distinguish them from one another by their behavior at infinity and studying the real part Eq. (2.68)

$$\mp\partial_t \log(\rho) = \sigma_r \cos(\sigma_\phi + 2\theta^0) + \lambda_r \cos(\lambda_\phi + 4\theta^0)\rho^2\,. \tag{2.79}$$

In this case ($\rho \to \infty$ for large negative flow times), we use Eq. (2.77) and we approximate

$$\mp\partial_t \log(\rho) = \mp\frac{\partial_t \rho}{\rho(t)} \approx \lambda_r \cos(n\pi)\rho^2 = (-1)^n \lambda_r \rho^2\,.$$

Assuming $\frac{d\rho}{dt} < 0$ in the large negative t limit, we identify even n with stable extended thimbles. Extended thimbles can therefore only connect to infinity in directions $\theta^0 = \frac{k\pi}{2}$ for $k \in \{0, 1, 2, 3\}$. These directions are centered in the upper defined regions Ω_i. Dual extended thimbles on the other hand are associated with odd n and can only connect to infinity in directions $\theta^0 = \frac{(2k+1)\pi}{4}$ for $k \in \{0, 1, 2, 3\}$

Fig. 2.3 shows this exact Lefschetz thimbles decomposition of the real line for the unmodified model and different σ. Thimbles are drawn as solid lines and their duals as dashed lines. The thimbles with non-zero cycle coefficients are drawn in blue, otherwise in gray. In the phase of broken symmetry ($Re\,\sigma < 0$) three thimbles are present in the decomposition. In the symmetric phase ($Re\,\sigma > 0$), a single relevant thimble is observed. We further note the key features described in this section which are also present in Fig. 2.3:

- Thimbles that connect a critical point to infinity do so in directions $\frac{k\pi}{2}$ for $k \in \{1, 2, 3, 4\}$
- Dual thimbles that connect a critical point to infinity do so in directions $\frac{(2k+1))\pi}{4}$ for $k \in \{1, 2, 3, 4\}$
- Thimbles that connect to a critical point with a finite point do so in directions $\frac{n\pi - \lambda_\phi}{4} = \frac{m\pi - \sigma_\phi}{2}$ for some $m, n \in \mathbb{Z}$

The first two properties are observed in all three scenarios at hand and is independent of the real part of σ. The third property is visible in bottom plot, where a thimble connects the critical point at zero with two critical points in directions

Die approbierte gedruckte Originalversion dieser Diplomarbeit ist an der TU Wien Bibliothek verfügbar
The approved original version of this thesis is available in print at TU Wien Bibliothek.
TU Bibliothek Your knowledge hub WIEN

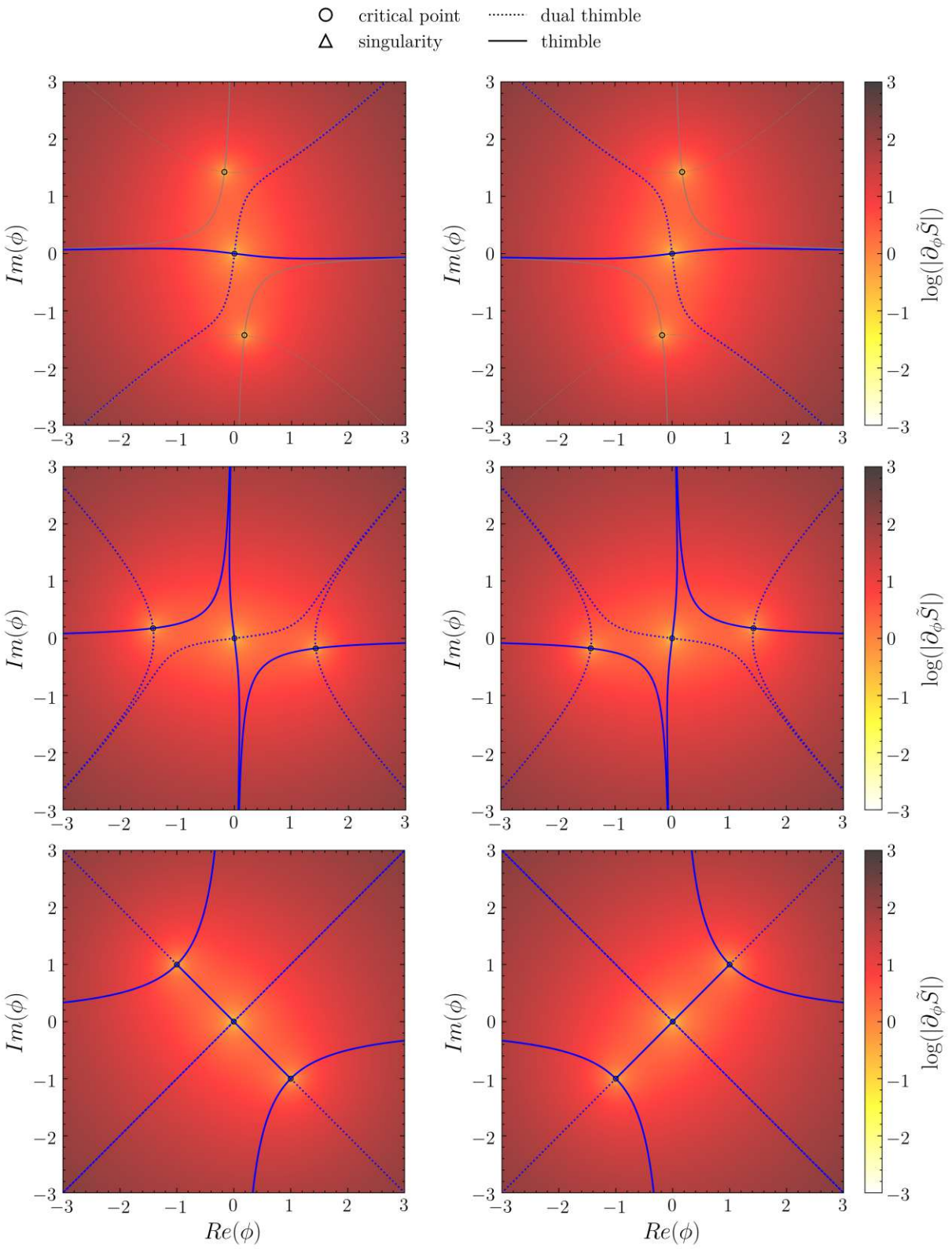

Fig. 2.3: The Lefschetz thimbles of the unmodified theory are shown for different mass parameters σ. The upper panels show how multiple thimbles are relevant in the phase of broken symmetry (left: $\sigma = -4 + i$, right: $\sigma = -4 - i$). The middle panels show that a single thimble is relevant in the phase of unbroken symmetry (left: $\sigma = 4 + i$, right: $\sigma = 4 - i$). The lower panels show the transition between the two regimes (left: $\sigma = +i$, right: $\sigma = -i$). Relevant thimbles/dual-thimbles are drawn in blue, non-relevant thimbles/dual-thimbles are drawn in gray. $\lambda = 2$ was used.

Die approbierte gedruckte Originalversion dieser Diplomarbeit ist an der TU Wien Bibliothek verfügbar
The approved original version of this thesis is available in print at TU Wien Bibliothek.
TU Bibliothek Your knowledge hub WIEN

To close the discussion of the thimble structure of the unmodified ϕ^4 model, we want to study the curvature of the critical points. These are determined by $\partial_z S = \sigma z + \lambda z^3 = 0$

$$z_0 = 0\,, \qquad z^{\pm} = \pm\sqrt{-\frac{\sigma}{\lambda}} = \sqrt{\frac{\sigma_r}{\lambda_r}} e^{i(\sigma_\phi - \lambda_\phi \pm \pi)/2}\,.$$

Using the curvature $\partial_z^2 S = \sigma + 3\lambda z^2$, we classify critical points into attractive/repulsive.

$$z_0: \qquad \mathrm{Re}(\partial_z^2 S) = \sigma_r \cos(\sigma_\phi)\,, \tag{2.80}$$

$$z^{\pm}: \qquad \mathrm{Re}(\partial_z^2 S) = \sigma_r \cos(\sigma_\phi) + 3\sigma_r \cos(\sigma_\phi - \lambda_\phi \pm \pi)\,. \tag{2.81}$$

z_0 changes from attractive to repulsive at $\sigma_\phi \in \left\{\frac{\pi}{2}, \frac{3\pi}{2}\right\}$ $z^{\pm}$ will change its curvature at

$$\cos(\sigma_\phi) = 3\cos(\sigma_\phi - \lambda_\phi) \tag{2.82}$$

For real coupling ($\lambda_\phi \in \{0, \pi\}$) we find a change of curvature in $z^{\pm}$ for $\sigma_\phi \in \{\frac{\pi}{2}, \frac{3\pi}{2}\}$. For generic coupling $\lambda_\phi \in (0, 2\pi)$ the behavior changes at

$$\sigma_\phi = \frac{3\sin(\lambda_\phi)}{3\cos(\lambda_\phi) - 1}\,. \tag{2.83}$$

2.4.2 Modified Theory

We now consider a modification of the scalar model discussed previously. The action is given as

$$S: \mathbb{R} \to \mathbb{C}, \quad S(x) = \frac{\sigma}{2}x^2 + \frac{\lambda}{4}x^4, \quad \sigma \in \mathbb{C}, \lambda \in \mathbb{R}\,. \tag{2.84}$$

In the CL method, we use the analytically continued function of S, which we denote by the same letter

$$S: \mathbb{C} \to \mathbb{C}, \quad S(\phi) = \frac{\sigma}{2}\phi^2 + \frac{\lambda}{4}\phi^4, \quad \sigma \in \mathbb{C}, \lambda \in \mathbb{R}\,. \tag{2.85}$$

For a given action, the non-normalized probability density is defined as

$$\rho: \mathbb{C} \to \mathbb{C}, \quad \rho(\phi) = \exp[-S(\phi)]\,. \tag{2.86}$$

As discussed earlier, a single thimble is relevant in the regime of unbroken symmetry ($\Re\sigma > 0$) and multiple thimbles are relevant in the regime of broken symmetry ($\Re\sigma < 0$). This may restrict the applicability of CL to certain regimes of the parameter space.

To overcome this limitation, we consider a modified theory defined by adding a holomorphic function $rR(\phi)$ to the original density

$$\tilde{\rho}(\phi) = \rho(\phi) + rR(\phi) \tag{2.87}$$

where $r \in \mathbb{R}$ is the strength of the modification. We refer to r as the *pullback* and $R(\phi)$ as the *density modification*.

It is instructive to examine the two limits of $|r| \to 0$ and $|r| \to \infty$. A vanishing value of r recovers the unmodified theory determined by ρ while big magnitudes of r give a theory only

Die approbierte gedruckte Originalversion dieser Diplomarbeit ist an der TU Wien Bibliothek verfügbar
The approved original version of this thesis is available in print at TU Wien Bibliothek.

determined by the density modification. In analogy to the modified density, we define the modified action $\tilde{S} = S + \psi$ and enforce the condition $\tilde{\rho} = \exp[-\tilde{S}]$. This leads to

$$\psi = -\ln[1 + rR(\phi)\, \exp(S)]\,. \tag{2.88}$$

To study thimble structure of the modified theory, we consider the complex derivative of the modified action and find

$$\partial_\phi \tilde{S} = \partial_\phi S - \frac{\partial_\phi [rR(\phi)\, \exp(S)]}{1 + rR(\phi)\, \exp(S)}\,. \tag{2.89}$$

Assuming an exponential ansatz $R = \exp \xi(\phi)$, we find that ξ acts additive on the unmodified action

$$\partial_\phi \tilde{S} = \partial_\phi S - \frac{r\, \exp[S(\phi) + \xi(\phi)]}{1 + r\, \exp[S(\phi) + \xi(\phi)]} \partial_\phi (S(\phi) + \xi(\phi))\,. \tag{2.90}$$

A concrete and analytically tractable choice is $\xi(\phi) = -\frac{\alpha}{2}\phi^2$ with $\alpha \in \mathbb{R}$ corresponding to a Gaussian modification and the resulting derivative

$$\partial_\phi \tilde{S} = \partial_\phi S - \frac{re^{\Sigma}}{1 + re^{\Sigma}} \partial_\phi \Sigma \tag{2.91}$$

where we introduced the mass-modified action

$$\Sigma := \Sigma(\phi) = S(\phi)\big|_{\sigma \to \sigma - \alpha} = \frac{\sigma - \alpha}{2}\phi^2 + \frac{\lambda}{4}\phi^4\,. \tag{2.92}$$

Remarkably, this derivative can be expressed only in terms of this mass-modified action

$$\partial_\phi \tilde{S} = \partial_\phi (\Sigma - \xi) - \frac{re^{\Sigma}}{1 + re^{\Sigma}} \partial_\phi \Sigma \tag{2.93}$$

$$= -\partial_\phi \xi + \partial_\phi \Sigma \left[1 - \frac{re^{\Sigma}}{1 + re^{\Sigma}}\right] \tag{2.94}$$

$$= -\partial_\phi \xi + \frac{\partial_\phi \Sigma}{1 + re^{\Sigma}}\,. \tag{2.95}$$

We aim to analyze the Lefschetz thimble structure of the Gaussian-modified model. As discussed in Chapter 2.4, the thimble connects a critical point to either another critical point, a singularity, or infinity. This follows from the monotonicity of the real part of the action along the thimble. If the action contains a non-removable singularity at ϕ_0, its derivative must also exhibit a singularity at ϕ_0. The singularities in the drift are located at ϕ that solve $1 + re^{\Sigma} = 0$. This condition gives the fourth-order polynomial equation

$$\frac{\sigma - \alpha}{2}\phi^2 + \frac{\lambda}{4}\phi^4 + 2\pi i\, n + \ln(-r) = 0 \tag{2.96}$$

Die approbierte gedruckte Originalversion dieser Diplomarbeit ist an der TU Wien Bibliothek verfügbar
The approved original version of this thesis is available in print at TU Wien Bibliothek.

whose solutions are given by

$$\phi_1^{\pm} = +\sqrt{\frac{0.5(\alpha-\sigma) \pm \sqrt{0.25(\alpha-\sigma)^2 - \lambda(2\pi i\, n + -\ln(r))}}{0.5\lambda}}\,, \tag{2.97}$$

$$\phi_2^{\pm} = -\sqrt{\frac{0.5(\alpha-\sigma) \pm \sqrt{0.25(\alpha-\sigma)^2 - \lambda(2\pi i\, n + -\ln(r))}}{0.5\lambda}}\,. \tag{2.98}$$

These are potential endpoints of thimbles in the modified theory and we used them to verify the numerical integration scheme we implemented to solve the thimble flow equations. Solving the flow equations is essential to determine the number of relevant thimbles for a given set of modification parameters.

The critical points are solutions to $\partial_\phi \tilde{S} = 0$. Assuming the critical point is non-singular, we multiply by $1 + re^{\Sigma}$ and obtain

$$\begin{aligned} 0 &= -(\partial_\phi \xi)(1 + re^{\Sigma}) + \partial_\phi \Sigma && (2.99)\\ &= \alpha\phi + \alpha\phi r e^{\Sigma} + \partial_\phi \Sigma && (2.100)\\ &= \phi[\alpha r e^{\Sigma} + \sigma + \lambda\phi^2]\,. && (2.101) \end{aligned}$$

This gives the trivial critical point at $\phi = 0$. Additional critical points must solve the transcendental equation

$$0 = \alpha r \exp(\Sigma) + \sigma + \lambda\phi^2 \tag{2.102}$$

which can be solved numerically. Also these are used in the numerical integration of the flow equations: they can be used as initial conditions for a solution of the flow equations. We now point out some symmetry properties of the thimble structure. These symmetry properties were used to further verify the validity of the numerical integration schemes.

The modified action a inherits the $\mathbb{Z}_2$ symmetry. Let $\phi_\alpha^*(t)$ denote a solution to the downward flow equation

$$\overline{\frac{d\phi_\alpha^*(t)}{dt}} = \left(\partial_\phi \xi - \frac{\partial_\phi \Sigma}{1 + re^{\Sigma}}\right)_{\phi_\alpha^*(t)} \tag{2.103}$$

and let the fixed point condition $\lim_{t\to\infty} \phi_\alpha^*(t) = \alpha$ be fulfilled. We use the identities

$$\begin{aligned} &\Sigma(\phi) = \Sigma(-\phi)\,, && (2.104)\\ &\partial_\phi \Sigma(-\phi) = -\partial_\phi \Sigma(\phi)\,, && (2.105)\\ &\partial_\phi \xi(-\phi) = -\partial_\phi \xi(\phi)\,. && (2.106) \end{aligned}$$

And find that the drift is antisymmetric

$$\left(\partial_\phi \xi - \frac{\partial_\phi \Sigma}{1 + re^{\Sigma}}\right)_{\phi_\alpha^*(t)} = -\left(\partial_\phi \xi - \frac{\partial_\phi \Sigma}{1 + re^{\Sigma}}\right)_{-\phi_\alpha^*(t)}\,. \tag{2.107}$$

In Eq. (2.103) we may now flip the sign of $\phi_\alpha^*(t) \to -\phi_\alpha^*(t)$ and see that the flow equation remains unchanged. From this we conclude that if $\phi_\alpha^*(t)$ parametrizes a thimble then so does $-\phi_\alpha^*(t)$ with the fixed point changed from α to $-\alpha$.

The modified model omits a second discrete symmetry, up to complex conjugation of the mass parameter σ. Let $\phi_\alpha^*(t)$ again denote a solution of the downward flow equation. We now

Die approbierte gedruckte Originalversion dieser Diplomarbeit ist an der TU Wien Bibliothek verfügbar
The approved original version of this thesis is available in print at TU Wien Bibliothek.
TU Bibliothek Your knowledge hub WIEN

study the behavior of the flow under complex conjugation, that is, under the transformation $\phi^*_\alpha(t) \to \overline{\phi^*_\alpha(t)}$. Assuming real parameters $r, \lambda, \alpha \in \mathbb{R}$, we observe the following identities:

$$\Sigma(\overline{\phi}) = \overline{\Sigma(\phi;\, \sigma \to \overline{\sigma})}\,, \tag{2.108}$$

$$\partial_\phi \Sigma(\overline{\phi}) = \overline{\partial_\phi \Sigma(\phi;\, \sigma \to \overline{\sigma})}\,, \tag{2.109}$$

$$\partial_\phi \xi(\overline{\phi}) = \overline{\partial_\phi \xi(\phi)}\,. \tag{2.110}$$

From this, it follows that the drift transforms as

$$\partial_\phi \tilde{S}\big|_{\overline{\phi^*_\alpha(t)}} = \overline{\partial_\phi \tilde{S}\big|^{\sigma\to\overline{\sigma}}_{\phi^*_\alpha(t)}}\,. \tag{2.111}$$

This implies that the complex conjugate path $\overline{\phi^*_\alpha(t)}$ solves the downward flow equation of the theory with mass parameter $\overline{\sigma}$. In other words, the flow is equivariant under complex conjugation, provided the mass parameter is conjugated as well. The thimble structure is therefore symmetric under $\phi \to \overline{\phi}$, up to $\sigma \to \overline{\sigma}$.

Figures 2.4, 2.5 show the Lefschetz thimbles of the modified theory for different values of the mass parameter σ and the pullback r. The upper panels correspond to values of $r < r_c$ below a certain critical parameter r_c for which multiple thimbles are relevant, while in the lower panels, $r > r_c$ has been increased beyond a critical value r_c (see Chapter 4.3 for a detailed discussion of r_c), resulting in a single relevant thimble. The symmetry properties pointed out above are clearly manifest in the plots. First, the point symmetry, $\phi^*_\alpha(t) \mapsto -\phi^*_\alpha(t)$, is evident in the form of inversion symmetry about the origin throughout all plots. Second, the conjugation symmetry, $\phi^*_\alpha(t) \mapsto \overline{\phi^*_\alpha(t)}$, is visible when comparing the left and right panels: the values of σ used in the left panels are complex conjugates of those in the right panels, and the plots are mirror images reflected across the imaginary axis.

Die approbierte gedruckte Originalversion dieser Diplomarbeit ist an der TU Wien Bibliothek verfügbar
The approved original version of this thesis is available in print at TU Wien Bibliothek.
TU Bibliothek Your knowledge hub WIEN

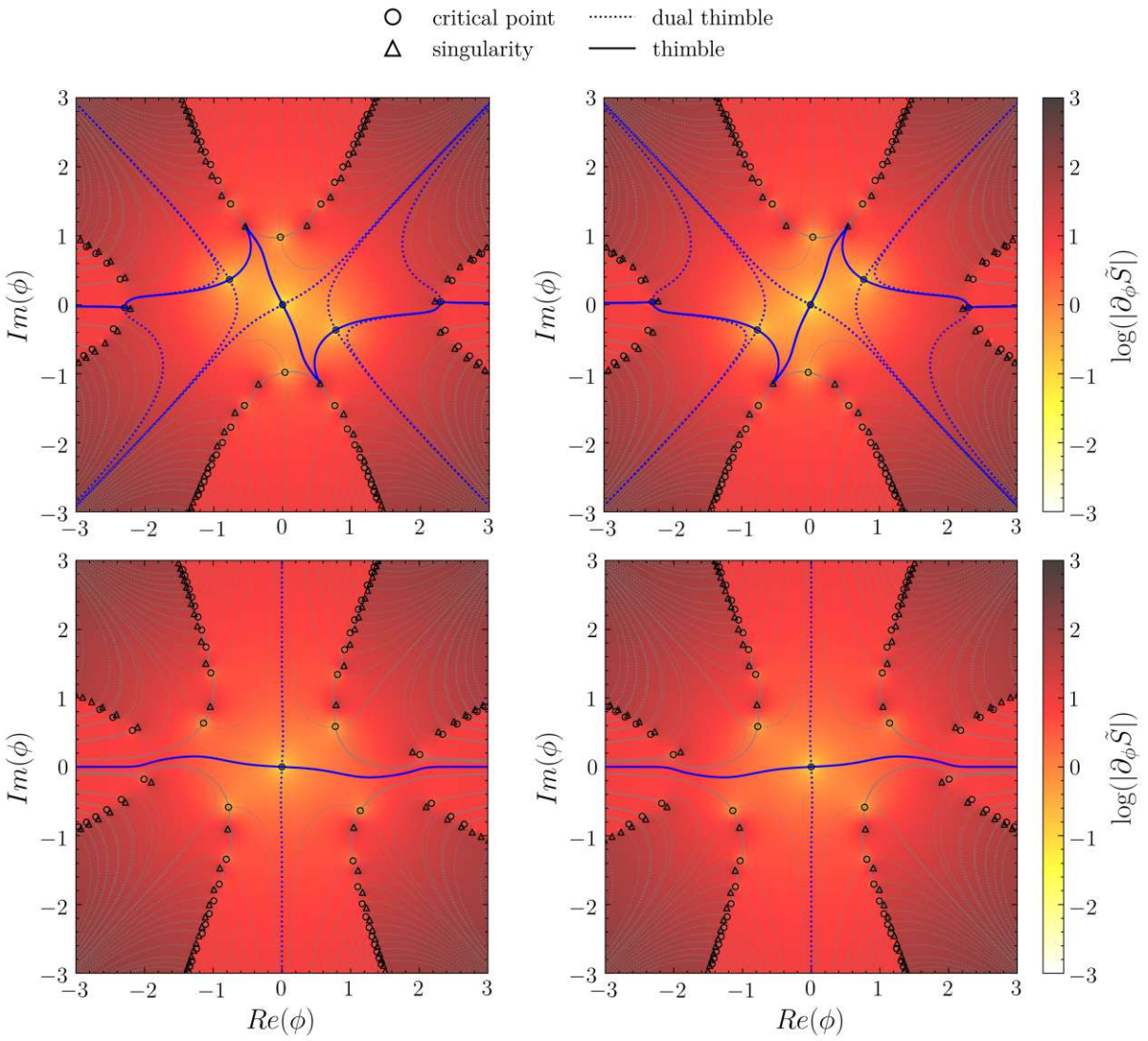

Fig. 2.4: The Lefschetz thimbles of the modified theory are shown for two different pullback parameters r. The upper plots show how multiple thimbles are relevant below a critical parameter r_c. Above r_c, a single thimble is relevant - even in the originally phase of broken symmetry. Relevant thimbles/dual-thimbles are drawn in blue, non-relevant thimbles/dual-thimbles are drawn in gray. $\sigma = -1 + i$ (left plots), $\sigma = -1 - i$ (right plots) and $\lambda = 2$ were used.

Die approbierte gedruckte Originalversion dieser Diplomarbeit ist an der TU Wien Bibliothek verfügbar
The approved original version of this thesis is available in print at TU Wien Bibliothek.

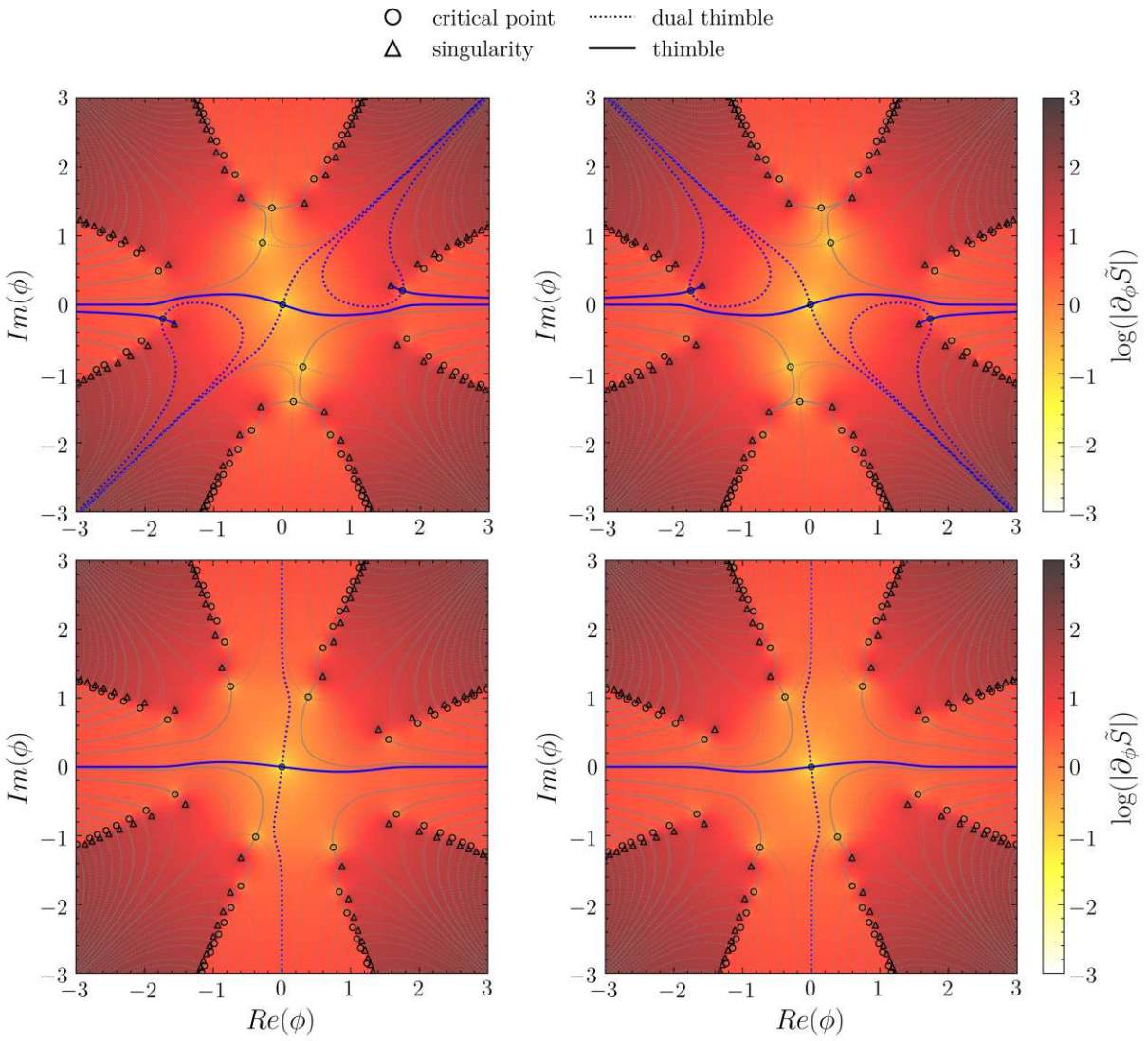

Fig. 2.5: The Lefschetz thimbles of the modified theory are shown for two different pullback parameters r. The upper plots show how multiple thimbles are relevant below a critical parameter r_c. Above r_c, a single thimble is relevant - even in the originally phase of broken symmetry. Relevant thimbles/dual-thimbles are drawn in blue, non-relevant thimbles/dual-thimbles are drawn in gray. $\sigma = +1 + i$ (left plots), $\sigma = +1 - i$ (right plots) and $\lambda = 2$ were used.

Die approbierte gedruckte Originalversion dieser Diplomarbeit ist an der TU Wien Bibliothek verfügbar
The approved original version of this thesis is available in print at TU Wien Bibliothek.

Chapter 3

Numerical Implementation

In this chapter, we discuss the numerical implementation of the CL simulations used throughout this thesis. Emphasis was placed on achieving computational efficiency via GPU acceleration using the CUDA framework. A significant portion of the implementation, specifically the interaction between Python and CUDA through the NUMBA library, was adapted from the work in [56].

3.1 Adaptive Stepsize

CL dynamics suffers from two major issues: runaway trajectories and wrong convergence [9, 17]. Although the latter may be more severe from a result-driven perspective, runaway trajectories can make simulations practically unusable. Runaway behavior arises when the dynamical degrees of freedom blow up, making numerical evolution unstable. As shown in [57, 58], this issue can be tamed by introducing an adaptive stepsize. The stepsize is dynamically computed at each iteration according to

$$\tilde{\epsilon} = \epsilon \frac{\langle K_{\max} \rangle}{K_{\max}}, \tag{3.1}$$

where ϵ is the constant stepsize and $K_{\max}$ denotes the current maximal drift magnitude (over all lattice points in field-theoretic simulations). The factor $\langle K_{\max} \rangle$ is a heuristic estimate of the typical drift in a metastable regime.

To compute statistically representative observables, one can generally use two strategies: (1) evolve a single trajectory over many Langevin steps and compute Langevin-time-averaged observables after thermalization, or (2) thermalize the simulation with different seeds and calculate observables across these in a smaller Langevin time span. Later, we will refer to the evolution in Langevin time starting with different seeds as different trajectories. The second approach was chosen here, because it is more amenable to run the simulation in parallel. However, treating observables from independent trajectories poses subtle challenges. Because the stepsize adapts dynamically, different trajectories evolve at different speeds through Langevin time. Consequently, synchronizing measurements across trajectories is problematic. Since observables should be sampled only after the system has become uncorrelated (i.e., after an *autocorrelation time*, see Chapter 3.2), naively aligning all trajectories in Langevin time can lead to inefficient implementations, particularly when a small stepsize slows down progress.

To resolve this, we implemented an asynchronous strategy compatible with parallel execution. After each simulation step, observables on each trajectory are labeled as either *cold* (sufficient Langevin time has passed since the last measurement, measurements are uncorrelated) or *hot* (not yet uncorrelated). *Cold* observables are then computed in parallel across all trajectories. This results in a form of asynchronous sampling: observables are measured at different Langevin times across the trajectories, and all the measurements are uncorrelated. However, this method introduces a survivorship bias. Since some trajectories evolve faster (due to larger average stepsize), they reach higher Langevin times earlier with respect to simulation time. In practice,

Die approbierte gedruckte Originalversion dieser Diplomarbeit ist an der TU Wien Bibliothek verfügbar
The approved original version of this thesis is available in print at TU Wien Bibliothek.
TU Bibliothek Your knowledge hub WIEN

this means that measurements at late Langevin times may be dominated by a subset of trajectories that sampled in low-drift regions, thus breaking ergodicity and potentially skewing statistics.

To mitigate this bias, a natural solution would be to discard measurements beyond a certain Langevin time reached by all trajectories. Alternatively, the simulation could be stopped only when all trajectories reach a common target time, essentially reintroducing synchronization at the end of the simulation. Instead, we adopt a more practical approach: trajectories that slow down excessively, defined as having an adaptive stepsize smaller than a fixed fraction of the base stepsize, are discarded. Specifically, we set a lower bound of $\tilde{\epsilon}/\epsilon < 10^{-3}$. This ensures that all remaining trajectories contribute evenly to the ensemble averages while preserving the advantages of asynchronous execution.

3.2 Autocorrelation

In general, the finite stepsize used in the discretized Langevin equation induces correlations over Langevin time. Once the process has thermalized, these correlations do not bias the expectation values of observables averaged over long Langevin time intervals. However, they do introduce a bias in the estimation of the variance of these observables [59]. To address this, the observables must be sampled sufficiently far apart in Langevin time to ensure statistical independence. A ruler for this time difference is the autocorrelation (Langevin) time. If samples are drawn only after their autocorrelation time has passed, the data points are independent, and statistics on the sample may be used to estimate the statistics of the population. Autocorrelated samples, on the other hand, may give wrong estimates for the statistics of the population. Figure 3.1 illustrates this point by comparing the evolution of a complex stochastic variable with zero mean under autocorrelated and decorrelated sampling. The effect on estimates on the standard error of the mean is clearly visible.

The autocorrelation time generally depends on the specific parameters of the simulation and should not be assumed to behave uniformly across different simulation parameters. Furthermore, it may vary significantly between different observables. To obtain reliable and unbiased estimates of observable means and their statistical uncertainties, the autocorrelation time should be measured individually for each observable under consideration. We define the autocorrelation function $R_{\mathcal{O}}(\tau)$ of an observable $\mathcal{O}$ at Langevin time θ as [56]

$$R_{\mathcal{O}}(\tau) = \frac{\langle (\mathcal{O}_\theta - \langle \mathcal{O}_\theta \rangle)\,(\mathcal{O}_{\theta+\tau} - \langle \mathcal{O}_{\theta+\tau} \rangle) \rangle}{\sigma_\theta \sigma_{\theta+\tau}} \approx \exp\left(-\tau / T_{\mathcal{O}}\right), \tag{3.2}$$

where σ_θ denotes the standard deviation of $\mathcal{O}$ at Langevin time θ, and $T_{\mathcal{O}}$ is the autocorrelation time, assumed to follow an exponential decay [56].

Figure 3.2 shows schematic plots of the autocorrelation function for the second moment of the unmodified theory with parameters $\sigma = 1 + 1j$ and $\lambda = 2$, a Langevin timestep $dt = 5 \cdot 10^{-4}$ and 1000 trajectories.

Due to the inherent stochasticity of the Langevin process, measuring the autocorrelation time from a single trajectory is insufficient. Instead, we consider the distribution of autocorrelation times across an ensemble of independent trajectories. This is made computationally feasible by the parallelized simulation framework employed throughout this work.

Die approbierte gedruckte Originalversion dieser Diplomarbeit ist an der TU Wien Bibliothek verfügbar
The approved original version of this thesis is available in print at TU Wien Bibliothek.
TU Bibliothek Your knowledge hub WIEN

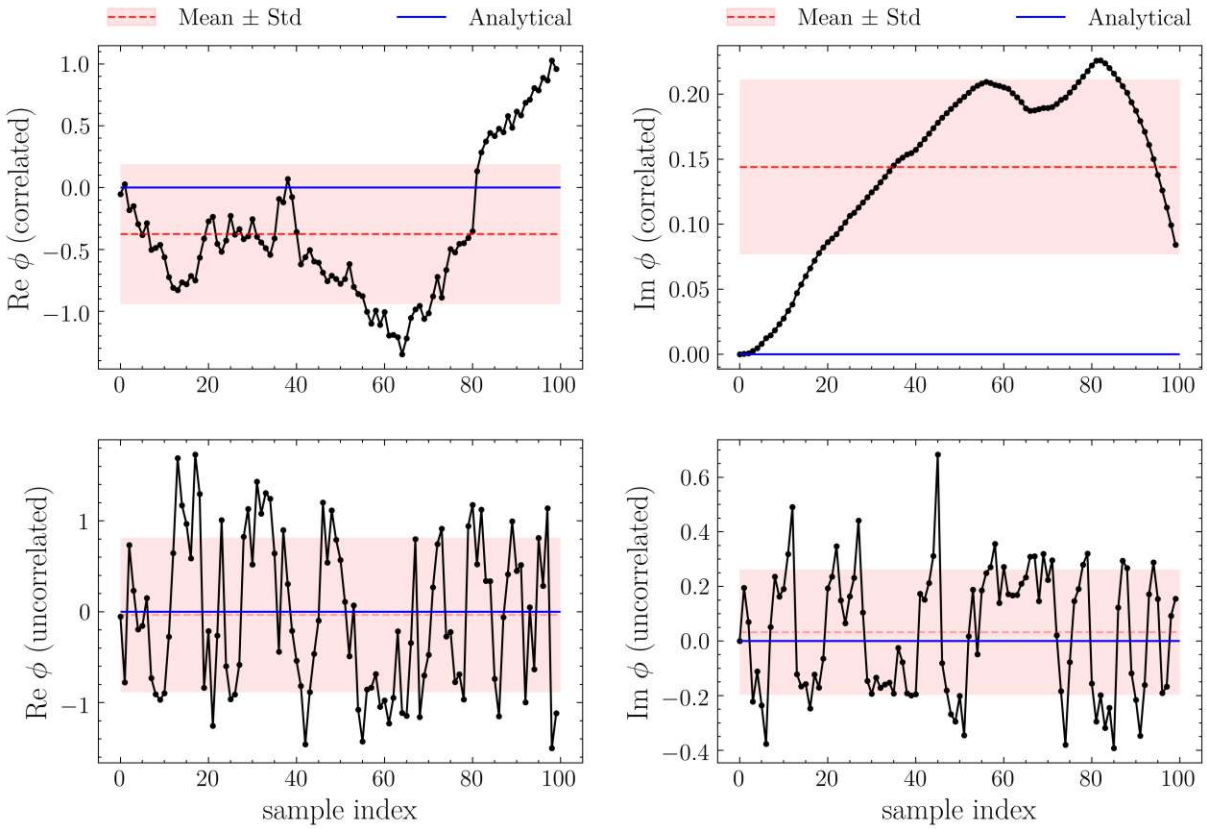

Fig. 3.1: Two trajectories of a complex stochastic variable with zero mean. In the upper panel, consecutive samples are taken at intervals shorter than the autocorrelation time, resulting in strong correlations and biased statistical estimators. In the lower panel, samples are taken only after sufficient time has passed, rendering them approximately independent.

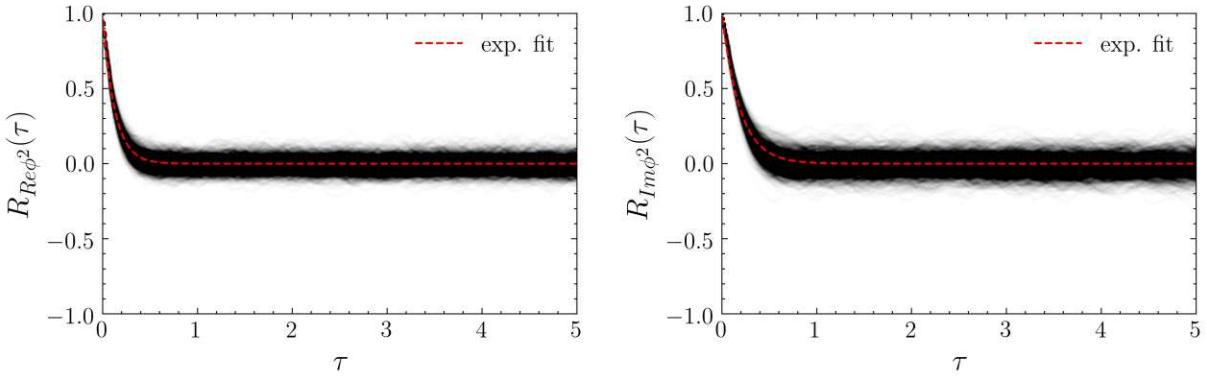

Fig. 3.2: Autocorrelation function $R_{\phi^2}(\tau)$ for the second moment of the unmodified theory with parameters $\sigma = 1 + 1j$, $\lambda = 2$, Langevin timestep $dt = 5 \cdot 10^{-4}$, and 1000 trajectories. The data is averaged over all trajectories to suppress noise, and an exponential fit is shown to extract the autocorrelation time T_{ϕ^2}.

Die approbierte gedruckte Originalversion dieser Diplomarbeit ist an der TU Wien Bibliothek verfügbar
The approved original version of this thesis is available in print at TU Wien Bibliothek.

3.3 Determination of drift histograms

As pointed out in section 2.3.2, drift histograms can be used to assess whether results obtained by CL are trustworthy. The criterion states that the distribution of the quantity $u := |\frac{\partial S}{\partial \phi}|$, which we refer to as the *drift histogram* must decay faster than any power of u for large u. This is a sufficient and necessary condition for the correctness of CL - even in the presence of meromorphic drift functions.

The most straight-forward way to estimate the drift histogram would surely be to consider the drift as an observable and calculate it in situ, i.e., during the simulation. However, this approach introduces several complications. First, it is impractical to store the full set of drift values. Assuming double-precision floats, an autocorrelation time of order one, a maximal Langevin time of 100, and 10^6 independent trajectories (or seeds), the storage required quickly reaches the order of 10^8 floating-point numbers, which corresponds to nearly a gigabyte of memory just for the drift data. For larger simulations or field-theoretic settings, this becomes prohibitive.

One might consider a more storage-efficient approach: binning the drift values on the fly and storing the resulting histograms. For this approach, we would first have to estimate the bin size needed and an upper bound of drift magnitudes - both of which are critical for correctly applying the decay criterion. In practice, this procedure turned out to be less convenient: the distribution of drift values spans several orders of magnitude, making it difficult to choose a fixed binning scheme that is both efficient and accurate. Instead, we employ a different method for calculating the drift histogram a posteriori, based on the histogram of the CL process itself. That is, we analyze the histogram of the scalar ϕ_c sampled during the CL process after the simulation has ended. We found it more feasible to estimate a reliable bounding region in the complex plane and choose a reasonable bin size there. Our goal is to infer the drift histogram $p(u)$ given a probability distribution $P(\phi_c)$ and an analytic expression for the drift $K = \partial S/\partial \phi_c$.
It is defined via

$$p(u) = \int d\phi_c \, P(\phi_c)\delta(u - |K(\phi_c)|) \, . \tag{3.3}$$

We assume the number of bins in the real and imaginary direction are equal and call it N. Then we estimate $P(\phi_c)$ via the histogram $H(\phi_c)$ which is a $N \times N$ matrix and approximate $p(u)$

$$p(u) \approx \sum_{\phi_c} H(\phi_R, \phi_I)\delta_{u,|K(\phi_c)|} \, , \tag{3.4}$$

where

$$\delta_{u,|K(\phi_c)|} = \begin{cases} 1 & u = |K(\phi_c)| \\ 0 & \text{else} \end{cases} \tag{3.5}$$

Quite simply, the approximation counts the number of points in the data set that satisfy $u = |K(\phi_c)|$ for a given u. A direct summation as in (3.4) would require us to calculate $\delta_{u,|K(\phi_c)|}$ $N^2 M$ times, where M is the resolution in u. In our case a typical choice would be $N = M = 10^3$. Using precompiled Python routines, we encountered typical execution times of the order $10^{-6}s$. Using this approach and these parameters, it would take on the order of 10min to calculate a single drift histogram. This would be acceptable for individual simulation runs, but it breaks the authors personal principle to *not let the echo outlive the voice - analyze faster than you simulate.* In that sense, we propose the following strategy:

Given a histogram $H(\phi_c) \in \mathbb{N}^{N\times N}$, that approximates the probability distribution $P(\phi_c)$ and the bounds in the complex plane $[\phi_R^{\min}, \phi_R^{\max}] \times [\phi_I^{\min}, \phi_I^{\max}]$. From this, discretize the domain

Die approbierte gedruckte Originalversion dieser Diplomarbeit ist an der TU Wien Bibliothek verfügbar
The approved original version of this thesis is available in print at TU Wien Bibliothek.
TU Wien Bibliothek Your knowledge hub

into an $N \times N$ grid of complex field values ϕ_c and compute the drift magnitude at each grid point:

$$K_{ij} = \left|K(\phi_c^{(i,j)})\right| = \left|\frac{\partial S}{\partial \phi_c}\Big|_{\phi_c^{(i,j)}}\right|$$

and store this as a matrix:

$$K = \begin{pmatrix} K_{00} & K_{01} & \cdots & K_{0(N-1)} \\ K_{10} & K_{11} & \cdots & K_{1(N-1)} \\ \vdots & \vdots & \ddots & \vdots \\ K_{(N-1)0} & K_{(N-1)1} & \cdots & K_{(N-1)(N-1)} \end{pmatrix}.$$

Using the histogram H, construct a flat dataset A of drift magnitudes, where each entry K_{ij} is included H_{ij} times:

$$A = \bigcup_{i,j} \{K_{ij}\}^{H_{ij}}. \tag{3.6}$$

That is, for each grid point (i, j), include K_{ij} in A with multiplicity H_{ij}. Choose the number of bins $M < N^2$ and a range $[u_{\min}, u_{\max}]$ covering the values in A. Construct the drift histogram by binning A into M intervals:

$$p(u) = \text{Histogram}(A; M, [u_{\min}, u_{\max}]).$$

This gives a binned estimate of the probability distribution of drift magnitudes.

Because the judgment of results we present in later sections will be based on drift histograms, we view it as essential to test this routine on an artificial dataset. For certain choices of $K(\phi_c)$, we find an analytical result for $p(u)$. We consider a $K(\phi_c)$ that is rotationally symmetric. In the first example, assume $K(\phi_c) = \sqrt{\phi_R^2 + \phi_I^2}$ and a uniform distribution in a circle C with radius R.

The normalized probability density is $P(\phi_c) = \frac{1}{R^2\pi}$ and $p(u)$ reduces to

$$p(u) = \int_C d\phi_c \, \frac{1}{R^2\pi} \delta(u - \sqrt{\phi_R^2 + \phi_I^2}) = \int_0^{2\pi} \int_0^R r dr d\phi \, \frac{1}{R^2\pi} \delta(u - r) = \frac{2u}{R^2}. \tag{3.7}$$

In the second example we consider the same drift $K(\phi_c) = \sqrt{\phi_R^2 + \phi_I^2}$ and a normal distribution in the complex plane. Using the density $P(\phi_c) = \frac{1}{2\pi} e^{-\frac{1}{2}(\phi_R^2 + \phi_I^2)}$, we get the closed form

$$p(u) = \int_{\mathbb{C}} d\phi_c \, \frac{1}{2\pi} e^{-\frac{1}{2}(\phi_R^2 + \phi_I^2)} \delta(u - \sqrt{\phi_R^2 + \phi_I^2}) = \int_0^{2\pi} \int_0^{\infty} r dr d\phi \, \frac{1}{2\pi} e^{-\frac{1}{2}r^2} \delta(u - r) = u e^{-\frac{1}{2}u^2}. \tag{3.8}$$

For both examples, we found good agreement between analytic expressions for $p(u)$ and simulated histograms. The results are shown in Fig. 3.3 and Fig. 3.4 for the uniform and gaussian distribution, respectively. The error bars were calculated on the basis of Poissonian statistics and the sampled data was fit to the analytical expressions (3.7) and (3.8) well. From this we conclude that the method of inferring the drift histogram a posteriori from a CL histogram works as expected.

Die approbierte gedruckte Originalversion dieser Diplomarbeit ist an der TU Wien Bibliothek verfügbar
The approved original version of this thesis is available in print at TU Wien Bibliothek.
TU Bibliothek Your knowledge hub WIEN

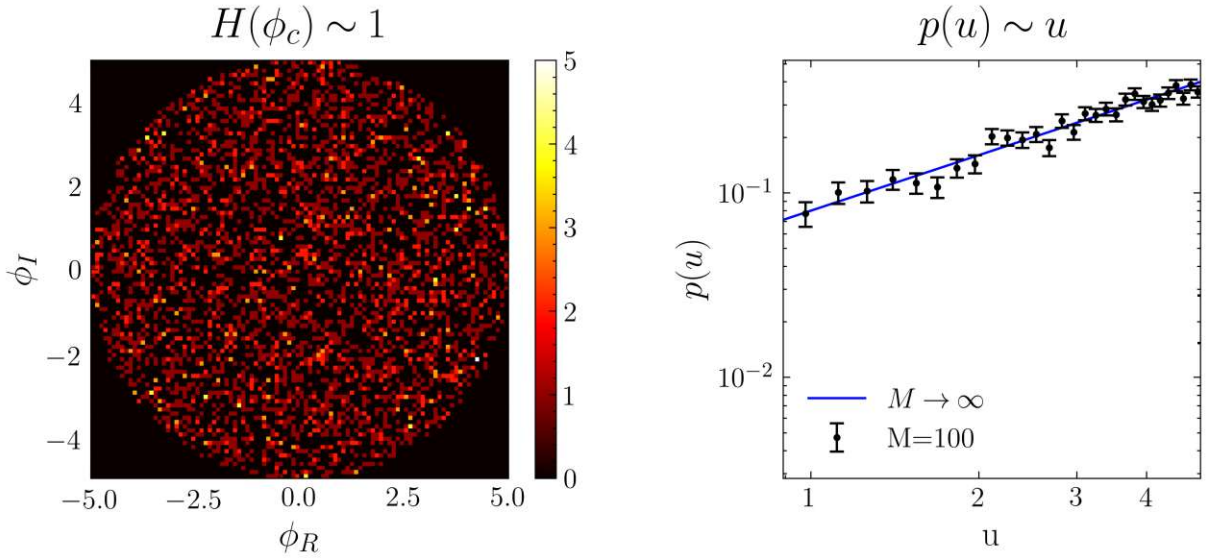

(a)

Fig. 3.3: Left panel: Histogram of a uniformly distributed variable in a circle of radius 5. The colorbar represents the relative occurrence in arbitrary units.
Right panel: associated histogram of the function $K(\phi_c) = \sqrt{\phi_R^2 + \phi_I^2}$. The number of bins M was set to 100.

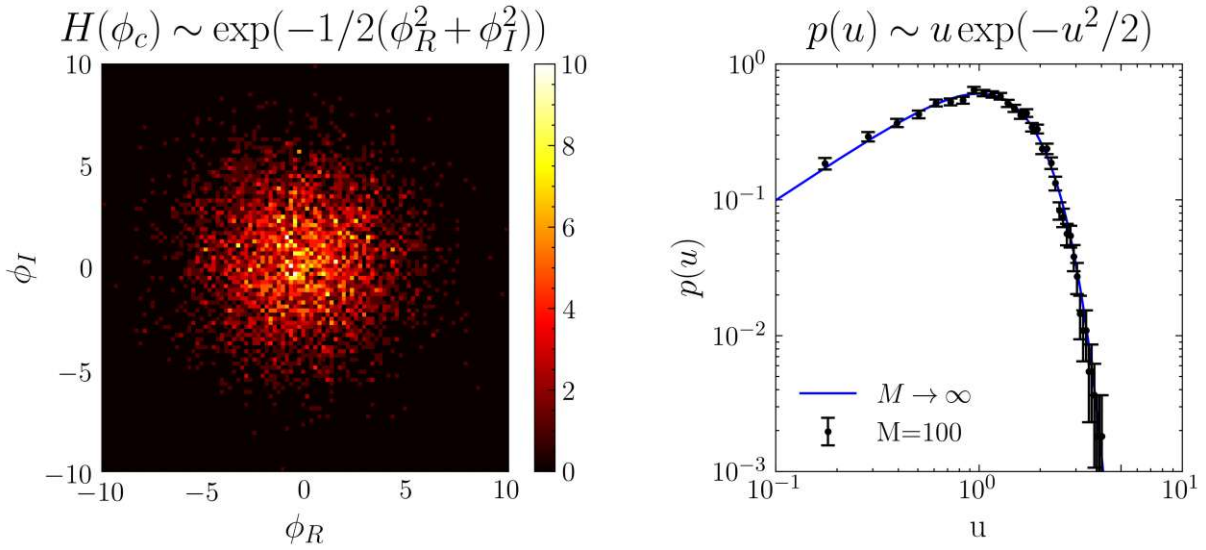

(a)

Fig. 3.4: Left panel: Histogram of a normally distributed random variable in the plane. The colorbar represents the relative occurrence in arbitrary units.
Right panel: associated histogram of the function $K(\phi_c) = \sqrt{\phi_R^2 + \phi_I^2}$. The number of bins M was set to 100.

Die approbierte gedruckte Originalversion dieser Diplomarbeit ist an der TU Wien Bibliothek verfügbar
The approved original version of this thesis is available in print at TU Wien Bibliothek.

Chapter 4

Results and Analysis

With the theoretical and numerical tools established, we now investigate how the geometry of the Lefschetz thimbles influences the convergence behavior of CL. We begin by analyzing the unmodified scalar model, identifying critical points and their associated thimbles, and comparing these with CL dynamics. We then apply modifications to the action designed to isolate or emphasize specific thimbles, studying their impact on the CL results and overall expectation values. This structure allows us to systematically explore the correspondence between thimble support and stochastic convergence.

4.1 Wrong convergence in the unmodified theory

We begin our analysis with the unmodified scalar model defined by the action $S(\phi)$ introduced in Eq. (2.2). This model exhibits a complex action in certain parameter regimes, including cases with complex mass parameter σ, which leads to a sign problem that renders standard Monte Carlo methods ineffective. The CL method offers a potential solution by extending the dynamics into the complexified field space. However, as we will demonstrate, the CL method does not always converge to the correct results. To understand the source of this failure, we show the geometry of the associated Lefschetz thimbles. In this section, we compare the observables obtained via CL with exact numerical results obtained through a standard quadrature integration routine and refer to these as "exact" values. We show that CL dynamics explores regions of the complexified field space with a density that breaks the criterion of correctness discussed in Chapter 2.3.2, leading to wrong convergence. This failure of the CL method sets the stage for introducing action modifications that aim to align the stochastic flow with a single relevant thimble. In the following, we focus on the first and second moments of the field to show that the CL process converges correctly or incorrectly.

Our CL simulations were performed for various values of σ in the upper half of the complex plane. The simulations used a Langevin step size of $5 \cdot 10^{-5}$, with $\lambda = 2$ and evolved 10^6 independent trajectories up to a maximal Langevin time of $\tau_{\max} = 100$. As discussed in Chapter 3.2, the autocorrelation time was measured in advance and found to be well below 2. After a thermalization time of $\tau_{\text{therm}} = 10$, observables were sampled every $\tau = 2$, corresponding to $2 \cdot 10^5$ steps between consecutive measurements.

Our main results are summarized in Fig. 4.1 and further detailed in Tables 4.1 and 4.2, where the real and imaginary parts of $\langle\phi\rangle$ and $\langle\phi^2\rangle$ are compared between the CL results and the "exact" values from standard quadrature routines. In the figure, we show the relative error of $\langle\phi^2\rangle$ obtained using CL as a function of the mass parameter σ for the fixed coupling $\lambda = 2$. The error is represented as a false-color plot in the $(|\sigma|, \arg(\sigma))$ plane. By showing the domains where the relative error becomes large, we illustrate the regions in the parameter space where CL converges wrongly. This visualization points out the strong dependence on the σ-phase for which the unmodified CL method is reliable. We find that in the regime of broken symmetry ($\text{Re}(\sigma) < 0$), CL does not converge correctly for different values of $|\sigma|$.

Die approbierte gedruckte Originalversion dieser Diplomarbeit ist an der TU Wien Bibliothek verfügbar
The approved original version of this thesis is available in print at TU Wien Bibliothek.
TU Bibliothek Your knowledge hub WIEN

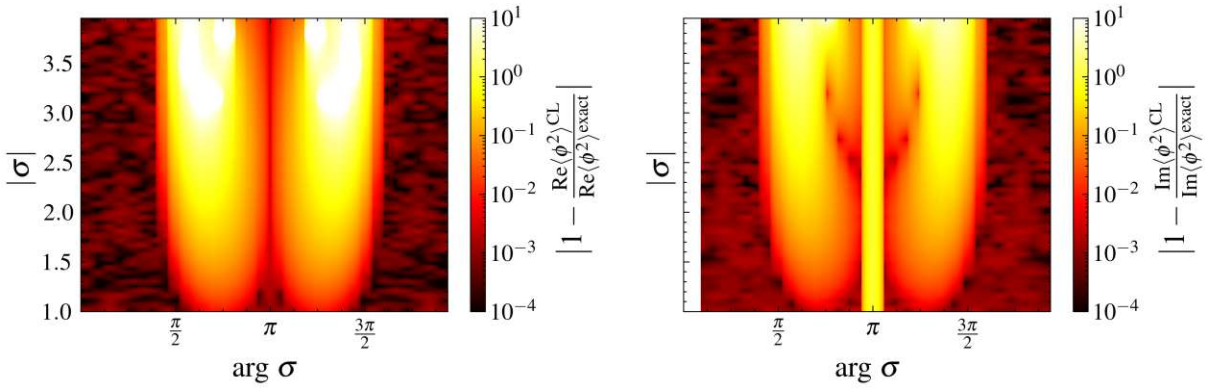

Fig. 4.1: Relative error of $\langle\phi^2\rangle$ obtained using CL in the unmodified theory with respect to the exact results. The data is shown as a function of the mass parameter σ in the $(|\sigma|, \arg(\sigma))$ plane. The color can be used as an indicator for wrong convergence.

This is further confirmed by Table 4.2, where one finds that in the regime of broken symmetry, the discrepancies between CL and the exact values are significant, especially as $|\sigma|$ is increased. The largest discrepancy appears for $\sigma = -1 + 4i$, where the CL result differs by a factor of 5 from the numerical value. Within the symmetric phase ($\mathrm{Re}(\sigma) > 0$), CL results for the second moment generally agree with the exact values up to discretization artifacts (see below). However, for certain regions of the mass parameters within the symmetric phase, we observe wrong convergence, confirming a previous study [40]. We will discuss this case in Chapter 4.2. We further observe that the first moment $\langle\phi\rangle$ agrees with the exact result of zero within three digits for all considered values of σ, which is seen in Table 4.1. The second moment deviates from the exact value by about 2% in the cases where expect correct convergence of CL. We note that these deviations between the CL and exact results originate from discretization artifacts introduced by the finite Langevin time step.

Figure 4.2 illustrates the CL process overlaid on the Lefschetz thimble structure of the unmodified theory. In the symmetric phase for $\sigma = 4 + i$ (upper panel), there is only a single relevant thimble, and the CL distribution appears well localized staying close to it. In contrast, in the broken phase for $\sigma = -4 + i$ (central panel), we find three relevant thimbles, and the CL dynamics explore a much wider region and do not remain close to any individual thimble. The drift histogram shown in the lower panel of this figure supports these statements: the case of $\sigma = 4 + i$ that we expect to have converged correctly indeed exhibits a rapidly decaying drift distribution, validating the drift-based criterion of correctness outlined in Chapter 2.3.2. On the other hand, the case of $\sigma = -4 + i$ that we expect to have converged incorrectly shows a long tail in the drift distribution and therefore the criterion is violated. We note that $\sigma = -4 + i$ is one of the parameter values included in Table 4.2, where the significant discrepancy between the CL and the exact result is consistent with this observed violation. In the case of $\sigma = +4 + i$, good agreement between the CL and the exact result was found in the same table. These findings further support the conjecture that correct CL convergence requires a single thimble to be relevant.

4.2 Bias correction method

The failure of the CL method (mostly) in the broken-symmetry phase is expected to be closely related to the presence of multiple relevant Lefschetz thimbles, as demonstrated in the previous

Die approbierte gedruckte Originalversion dieser Diplomarbeit ist an der TU Wien Bibliothek verfügbar
The approved original version of this thesis is available in print at TU Wien Bibliothek.
TU Bibliothek Your knowledge hub WIEN

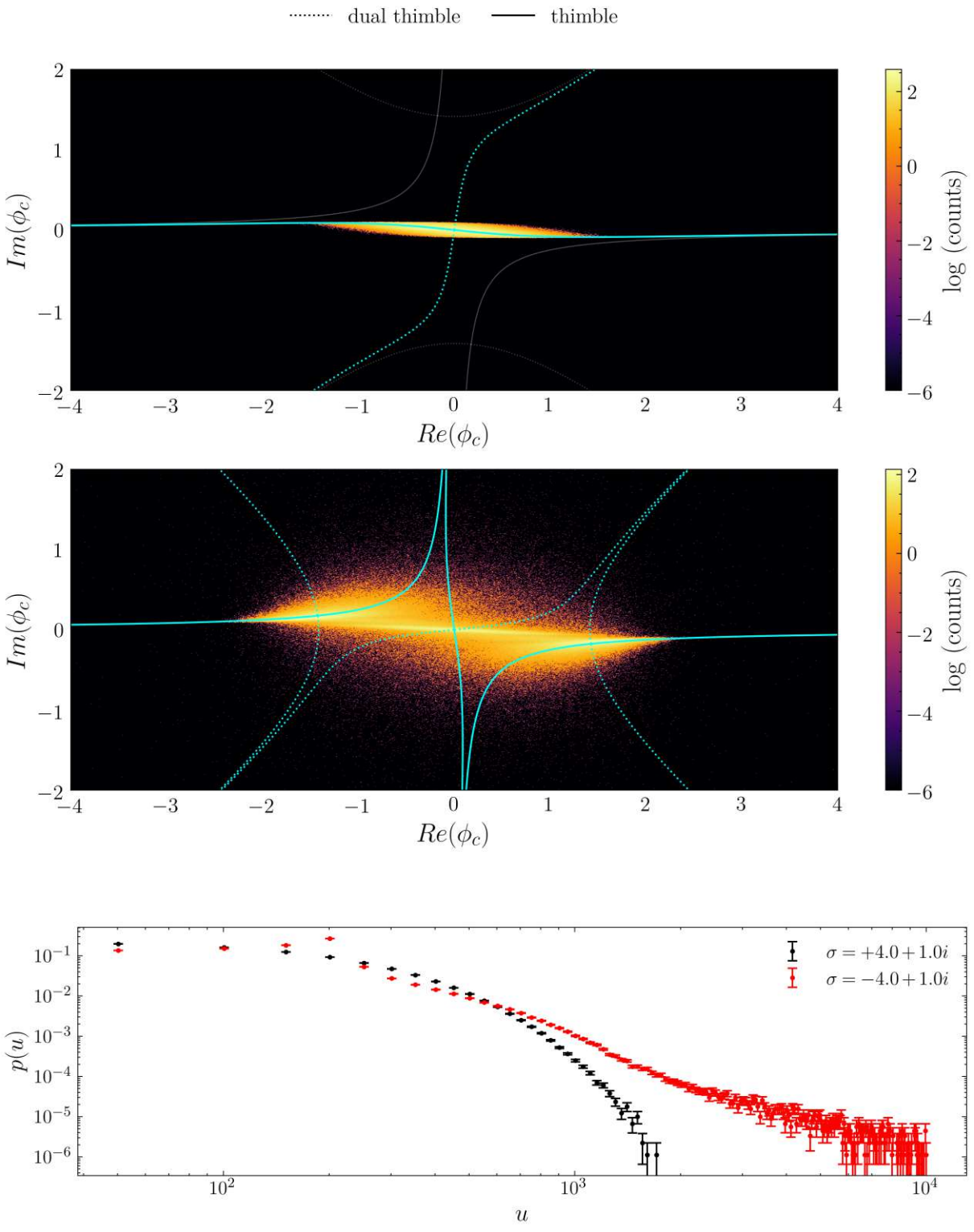

Fig. 4.2: CL sampling densities overlaid on Lefschetz thimbles for the unmodified theory with $\lambda = 2$. Top: For $\sigma = 4 + i$, only one thimble contributes, and CL dynamics remain localized, leading to correct convergence. Middle: For $\sigma = -4 + i$, multiple thimbles are relevant, and CL explores a wider region, causing wrong convergence. Bottom: Corresponding drift histograms. The correctly converging case shows rapid decay, while the incorrect case exhibits a long tail, violating the drift-based correctness criterion (see Chapter 2.3.2).

Die approbierte gedruckte Originalversion dieser Diplomarbeit ist an der TU Wien Bibliothek verfügbar
The approved original version of this thesis is available in print at TU Wien Bibliothek.
TU Bibliothek Your knowledge hub WIEN

σ	$\mathrm{Re}\langle\phi\rangle_\rho^{\mathrm{CL}}$	$\mathrm{Re}\langle\phi\rangle_\rho^{\mathrm{exact}}$	$\mathrm{Im}\langle\phi\rangle_\rho^{\mathrm{CL}}$	$\mathrm{Im}\langle\phi\rangle_\rho^{\mathrm{exact}}$
$-4+1i$	$-0.00054(5)$	0	$0.00014(5)$	0
$-3+1i$	$-0.00005(5)$	0	$0.00008(5)$	0
$-2+1i$	$0.00005(5)$	0	$0.00004(5)$	0
$-1+1i$	$0.00020(4)$	0	$-0.00001(4)$	0
$-1+2i$	$0.00002(7)$	0	$-0.00006(4)$	0
$-1+3i$	$0.0000(1)$	0	$-0.0000(1)$	0
$-1+4i$	$0.0001(1)$	0	$0.0000(1)$	0
$+4+1i$	$0.000085(8)$	0	$-0.000005(8)$	0
$+3+1i$	$0.00009(1)$	0	$-0.00001(1)$	0
$+2+1i$	$0.00010(1)$	0	$-0.00001(1)$	0
$+1+1i$	$0.00011(2)$	0	$-0.00001(2)$	0
$+1+2i$	$0.00010(3)$	0	$-0.00003(3)$	0
$+1+3i$	$0.00009(5)$	0	$-0.00004(5)$	0
$+1+4i$	$0.00007(7)$	0	$-0.00002(7)$	0

Tab. 4.1: Comparison of the first moment $\langle\phi\rangle$ computed using CL with exact results obtained from numerical quadrature, for the unmodified theory with action according to (2.2) and fixed coupling $\lambda = 2$. All values of $\langle\phi\rangle$ are consistent with zero within numerical precision, as expected from symmetry. The results exhibit small but statistically significant deviations for some values of σ, which we attribute to discretization artifacts arising from a finite Langevin stepsize.

section using specific examples. To restore correct convergence, we introduce a modification to the theory that enforces a single relevant thimble structure. The structure of the thimbles in the modified theory, introduced in chapter 2.4.2, shows that for suitable choices of the modification parameters (r, α), the integration contour can generally be deformed into a single thimble. This makes the modified theory a promising candidate for successful CL simulations.

More precisely, in the previous chapters, we have reviewed how the Lefschetz thimble decomposition of a real scalar model whose action (2.2) has a complex mass parameter σ and a real coupling λ is unique (a single relevant thimble) in the symmetric phase of $\mathrm{Re}(\sigma) > 0$ and non-unique (three contributing relevant thimbles) in the broken phase of $\mathrm{Re}(\sigma) < 0$. There is strong evidence that the correct convergence of CL is linked to the Lefschetz thimble structure of the theory. It was conjectured that a single relevant thimble associated with an attractive critical point may be enough to ensure the correctness of CL [21]. Counterexamples to this conjecture occur [40] if the noise is not real-valued or if the inequality

$$3\mathrm{Re}(\sigma)^2 > \mathrm{Im}(\sigma)^2 \tag{4.1}$$

does not hold, such that excursions towards $\pm i\infty$ become more probable and violate the convergence criterion. However, it may be possible to restore correct convergence using constant kernels, as suggested in related works [60, 61].

In this section, we employ a density modification to the cases where the original CL process fails to produce correct results. In general, the expectation values of the observables obtained in this modified theory no longer correspond directly to those of the original theory. Therefore, we present a bias correction scheme that allows us to recover observables of the unmodified theory

Die approbierte gedruckte Originalversion dieser Diplomarbeit ist an der TU Wien Bibliothek verfügbar
The approved original version of this thesis is available in print at TU Wien Bibliothek.
TU Bibliothek Your knowledge hub WIEN

σ	$\mathrm{Re}\langle\phi^2\rangle_\rho^{\mathrm{CL}}$	$\mathrm{Re}\langle\phi^2\rangle_\rho^{\mathrm{exact}}$	$\mathrm{Im}\langle\phi^2\rangle_\rho^{\mathrm{CL}}$	$\mathrm{Im}\langle\phi^2\rangle_\rho^{\mathrm{exact}}$
$-4+1i$	1.7782(1)	1.6672	−0.5012(1)	−0.5111
$-3+1i$	1.3041(1)	1.1897	−0.4172(1)	−0.4109
$-2+1i$	0.89903(9)	0.8394	−0.30325(9)	−0.2943
$-1+1i$	0.61187(5)	0.6048	−0.19967(5)	−0.1983
$-1+2i$	0.5651(1)	0.4850	−0.3996(1)	−0.3650
$-1+3i$	0.5353(2)	0.3010	−0.6284(2)	−0.4582
$-1+4i$	0.5163(3)	0.1069	−0.9073(3)	−0.4407
$+4+1i$	0.19271(1)	0.1926	−0.03247(1)	−0.0325
$+3+1i$	0.22900(1)	0.2289	−0.04406(1)	−0.0441
$+2+1i$	0.27867(1)	0.27858	−0.06164(1)	−0.06163
$+1+1i$	0.34880(2)	0.34870	−0.08894(2)	−0.08894
$+1+2i$	0.30058(3)	0.30049	−0.16270(3)	−0.16268
$+1+3i$	0.23220(5)	0.23208	−0.20906(5)	−0.20900
$+1+4i$	0.16350(8)	0.15982	−0.22785(8)	−0.22309

Tab. 4.2: Comparison of the second moment $\langle\phi^2\rangle$ computed using CL with exact results obtained from numerical quadrature, for the unmodified theory with action according to Eq.(2.2) and fixed coupling $\lambda = 2$. In the symmetric phase ($\mathrm{Re}(\sigma) > 0$), CL results generally agree with the exact values. In the broken phase ($\mathrm{Re}(\sigma) < 0$), however, significant deviations are observed, particularly at large $|\sigma|$, where multiple contributing thimbles lead to violations of the correctness criterion discussed in Chapter2.3.2. Small deviations in otherwise well-behaved cases are consistent with discretization artifacts due to the finite Langevin stepsize.

from simulations performed in the modified theory. The scheme was first mentioned in [21] and is here reformulated for the scalar model.

In particular, in order to study the effect of a single relevant thimble on the CL convergence behavior, we alter the theory by a holomorphic additive function in the density [21]

$$\rho(\phi_c) \to \rho(\tilde{\phi}_c) = \rho(\phi_c) + rR(\phi)\,, \tag{4.2}$$

where $r \in \mathbb{R}$ is a constant parameter that determines the strength of the modification. We refer to it as the *pullback* parameter, indicating the extent to which the modified theory is drawn away from the original theory. $R(\phi)$ is a holomorphic function in $L^1(\mathbb{C})$ on $\mathbb{C}$ that we call the density modification. The restriction to functions in $L^1(\mathbb{R})$ will become clear later. It is instructive to examine the two extrema of $|r| \to 0$ and $|r| \to \infty$. A vanishing value of r gives the unmodified theory determined by ρ, while large magnitudes of r give a theory dominated by the density modification itself. In analogy to the modified density, we define the modified action $\tilde{S} = S + \psi$ by using the condition $\tilde{\rho} = \exp[-\tilde{S}]$. This results in

$$\psi = -\ln[1 + rR(\phi)\,\exp(S)]\,.$$

Since the observables computed from $\tilde{\rho}$ generally differ from those of the original theory, we require a correction strategy. In [18, 21] this was done for a model defined on a compact domain.

Die approbierte gedruckte Originalversion dieser Diplomarbeit ist an der TU Wien Bibliothek verfügbar
The approved original version of this thesis is available in print at TU Wien Bibliothek.
TU Bibliothek Your knowledge hub WIEN

We want to apply the same approach here. A relation between observables with respect to different weights was identified as

$$Q := \frac{\langle \mathcal{O} \rangle_\rho - \langle \mathcal{O} \rangle_{\tilde{\rho}}}{\langle \mathcal{O} \rangle_{\tilde{\rho}} - \langle \mathcal{O} \rangle_R} = \frac{Z_R}{Z_\rho}\,, \tag{4.3}$$

with $Z_R = \int d\phi\, R(\phi)$, $\quad Z_\rho = \int d\phi\, \rho(\phi)$, $\quad \langle \mathcal{O} \rangle_R = 1/Z_R \int d\phi\; R(\phi)\mathcal{O}(\phi)$. The key point to note is that Q is an observable-independent quantity. If Q is known, it can be used to correct for the bias introduced by the modification

$$\langle \mathcal{O} \rangle_\rho = \langle \mathcal{O} \rangle_{\tilde{\rho}} + \Delta\,, \text{ with } \Delta = Q(\langle \mathcal{O} \rangle_{\tilde{\rho}} - \langle \mathcal{O} \rangle_R)\,. \tag{4.4}$$

This strategy allows to retrieve observables of the unmodified theory through CL simulations in the modified theory.

The ratio Q can be obtained by constructing an observable that vanishes with respect to ρ, $\langle \mathcal{O} \rangle_\rho = 0$. This allows to determine Q from CL simulations in the modified theory only,

$$Q = \frac{\langle \mathcal{O} \rangle_{\tilde{\rho}}}{\langle \mathcal{O} \rangle_R - \langle \mathcal{O} \rangle_{\tilde{\rho}}}\,. \tag{4.5}$$

To this end, we follow the strategy outlined in Ref. [21] and study observables that satisfy the Schwinger-Dyson equations of the form

$$\mathcal{O}^*_n = n\phi^{n-1} - \phi^n(\sigma\phi + \lambda\phi^3), \text{ with } n \in \mathbb{Z}\,. \tag{4.6}$$

Their expectation value according to the density

$$\rho \propto \exp\left(-\frac{\sigma}{2}\phi^2 - \frac{\lambda}{4}\phi^4\right) \tag{4.7}$$

is given by

$$\langle \mathcal{O}^*_n \rangle_\rho = \int_{-\infty}^{\infty} d\phi\, e^{-\frac{\sigma}{2}\phi^2 - \frac{\lambda}{4}\phi^4} \left[n\phi^{n-1} - \phi^n(\sigma\phi + \lambda\phi^3)\right]\,. \tag{4.8}$$

Due to the anti-symmetry of the integrand, we find that

$$\langle \mathcal{O}^*_{2n} \rangle_\rho = 0 \quad \text{for all } n \in \mathbb{Z}. \tag{4.9}$$

To show that $\langle \mathcal{O}^*_n \rangle_\rho$ also vanishes for odd n, we start with the expression

$$-\langle \phi^{2n+1}(\sigma\phi + \lambda\phi^3) \rangle_\rho = -\int_{-\infty}^{\infty} d\phi\, \phi^{2n+1}(\sigma\phi + \lambda\phi^3) e^{-\frac{\sigma}{2}\phi^2 - \frac{\lambda}{4}\phi^4}\,. \tag{4.10}$$

Because it involves a derivative of the action $S = \frac{\sigma}{2}\phi^2 + \frac{\lambda}{4}\phi^4$, we can rewrite this as

$$-\langle \phi^{2n+1}(\sigma\phi + \lambda\phi^3) \rangle_\rho = \int_{-\infty}^{\infty} d\phi\, \phi^{2n+1} \partial_\phi e^{-S(\phi)}\,. \tag{4.11}$$

Die approbierte gedruckte Originalversion dieser Diplomarbeit ist an der TU Wien Bibliothek verfügbar
The approved original version of this thesis is available in print at TU Wien Bibliothek.
TU Bibliothek Your knowledge hub WIEN

This can be partially integrated, and if and only if $\mathrm{Re}(\lambda) > 0$, the integrand vanishes at the boundary, yielding

$$-\langle\phi^{2n+1}(\sigma\phi+\lambda\phi^3)\rangle_\rho = -\int_{-\infty}^{\infty} d\phi\, e^{-S(\phi)}\partial_\phi\phi^{2n+1} \tag{4.12}$$

$$= -\int_{-\infty}^{\infty} d\phi\, e^{-S(\phi)}(2n+1)\phi^{2n} \tag{4.13}$$

$$= -\langle(2n+1)\phi^{2n}\rangle_\rho\,. \tag{4.14}$$

Adding $\langle(2n+1)\phi^{2n}\rangle_\rho$ on both sides shows that $\langle\mathcal{O}^*_{2n+1}\rangle_\rho$ indeed vanishes for all $n\in\mathbb{Z}$:

$$\begin{aligned} 0 &= \langle\phi^{2n+1}(\sigma\phi+\lambda\phi^3)\rangle_\rho - \langle(2n+1)\phi^{2n}\rangle_\rho \\ &= \langle\mathcal{O}^*_{2n+1}\rangle_\rho\,. \end{aligned} \tag{4.15}$$

This result also follows directly from the Dyson-Schwinger equations [26].

In the calculation of Q, we come across a term

$$\langle\mathcal{O}^*_n\rangle_R = \frac{1}{\int_{-\infty}^{+\infty} d\phi\, R(\phi)}\int_{-\infty}^{+\infty} d\phi\, R(\phi)\mathcal{O}^*_n\,. \tag{4.16}$$

We will argue below (see Eq. (4.22)) that a Gaussian modification $rR(\phi) = r\exp\left(-\frac{\alpha}{2}\phi^2\right)$ is suitable for our case, which fulfills the requirement $|\int_{-\infty}^{+\infty} d\phi\,\phi^n R(\phi)| < \infty$, for all $n\in\mathbb{N}_0$. For this modification, we can give an analytic expression for $\langle\mathcal{O}^*_n\rangle_R$. First, note that

$$\int_{-\infty}^{\infty} d\phi\,\phi^n R(\phi) = \begin{cases} \sqrt{\frac{2\pi}{\alpha}}\,\frac{1}{\alpha^{n/2}}(n-1)!! & \text{if } n \text{ even} \\ 0 & \text{if } n \text{ odd} \end{cases} \tag{4.17}$$

and

$$\int_{-\infty}^{+\infty} d\phi\, R(\phi) = \sqrt{\frac{2\pi}{\alpha}}\,. \tag{4.18}$$

Since $\mathcal{O}^*_{2n}$ contains only odd powers of ϕ, it follows by anti-symmetry that

$$\langle\mathcal{O}^*_{2n}\rangle_R = 0\,. \tag{4.19}$$

From here on, we assume $m = 2n+1$ is an odd integer and evaluate:

$$\langle\mathcal{O}^*_m\rangle_R = \frac{m(m-2)!!}{a^{(m-1)/2}} - \sigma\frac{m!!}{a^{(m+1)/2}} - \lambda\frac{(m+2)!!}{a^{(m+3)/2}}\,. \tag{4.20}$$

Hence, once $\langle\mathcal{O}^*_m\rangle_{\tilde\rho}$ is measured via CL in the modified theory, Q can be determined analytically via

$$Q = \frac{\langle\mathcal{O}^*_m\rangle_{\tilde\rho}}{\frac{m(m-2)!!}{a^{(m-1)/2}} - \sigma\frac{m!!}{a^{(m+1)/2}} - \lambda\frac{(m+2)!!}{a^{(m+3)/2}} - \langle\mathcal{O}^*_m\rangle_{\tilde\rho}}\,, \tag{4.21}$$

allowing unbiased reconstruction of observables in the original theory.

Die approbierte gedruckte Originalversion dieser Diplomarbeit ist an der TU Wien Bibliothek verfügbar
The approved original version of this thesis is available in print at TU Wien Bibliothek.
TU Bibliothek Your knowledge hub WIEN

4.3 Modification towards a single relevant thimble

In this section, we want to go into details about the additive density modification that can be used to restore the correct CL convergence. Five key considerations guided our decision on the form of the modification:

- **Integrability:** In order to determine the bias on observables introduced by the modification, a modification $R(\phi)$ has to fulfill $|\int_{\mathbb{R}} d\phi\, \phi^n R(\phi)| < \infty$.
- **Preservation of $\mathbb{Z}_2$ symmetry:** The unmodified theory is invariant under $\phi \to -\phi$. This symmetry ensures that all critical points and their associated thimbles are symmetrically arranged in the complexified field space, maintaining the vanishing of odd moments and simplifying the structure of the thimble decomposition.
- **Correct asymptotic behavior:** In compact domains, singularities are introduced at the domain boundaries to enforce a compact thimble structure [21]. In the present non-compact case, the correct behavior at infinity is achieved by ensuring integrability without introducing new singularities at finite field values. Thus, the requirement of controlled asymptotic behavior is already covered by the integrability condition.
- **Single attractive critical point:** The critical point associated with the single relevant thimble should be attractive [21].
- **Analytical results:** It is more convenient if some intermediate steps that are necessary to perform the bias correction can be computed analytically.

The Gaussian modification

$$rR(\phi) = r \exp\left(-\frac{\alpha\phi^2}{2}\right) \tag{4.22}$$

is a promising candidate that satisfies all of the criteria above. However, the precise choice of parameters (r, α) required to ensure that the modified theory has a single relevant thimble remains unknown. On the one hand, there may exist a critical value r_c that separates a regime with multiple relevant thimbles from a regime where only a single thimble is relevant. This value therefore sets a lower bound on r for successful modification. On the other hand, excessively large values of r may compromise the effectiveness of the bias correction method described in Chapter 4.2. There, the correction factor Q is determined analytically via Eq. (4.21) and relies on the numerical evaluation of the observable $\langle \mathcal{O}^* m \rangle_{\tilde{\rho}}$ using CL. Crucially, this method depends on the ability to statistically distinguish $\langle \mathcal{O}^m \rangle_{\tilde{\rho}}$ from the purely Gaussian expectation $\langle \mathcal{O}^m \rangle_R$. In the limit $r \to \infty$, the modification dominates the theory, and we get $\langle \mathcal{O}_m \rangle_{\tilde{\rho}} \to \langle \mathcal{O}_m \rangle_R$, making the correction undefined due to a vanishing denominator (c.f., Eq. (4.5)). Therefore, the method is only applicable in a finite window above r_c, where a single thimble is relevant, but statistical distinguishability between the two expectation values is still maintained. For a visual representation of the thimble structure of the modified theory, see Fig. 2.4 and Fig. 2.5. It shows how a single thimble becomes relevant above a critical pullback value r_c.

Furthermore, we can assume that the critical parameter r_c depends on the mass parameter σ and the coupling constant λ. Using a simple bisection algorithm, we identified the critical boundary (r_c, α_c) in the (r, α) plane, which separates a single relevant thimble from a multi-relevant thimble regime. Here we had to assume that a single thimble is relevant for any pullback $r > r_c$. The bisection is based on a numerical evaluation of the intersection number, which is done by numerically integrating the flow equations (2.57) and (2.61). After integration, one

Die approbierte gedruckte Originalversion dieser Diplomarbeit ist an der TU Wien Bibliothek verfügbar
The approved original version of this thesis is available in print at TU Wien Bibliothek.
TU Bibliothek Your knowledge hub WIEN

simply counts the intersections of the dual thimble and the real axis. Algorithm 1 explains the bisection algorithm used to determine the critical parameters (r_c, α_c), and the results are shown in Table 4.3 for different σ. Only those critical parameters (r_c, α_c) corresponding to the minimal pullback are presented. Throughout all critical parameters, we found that the critical point located at the origin is attractive.

Algorithm 1 Determine critical pullback strength r_c for single-thimble dominance

Input: Mass parameter σ, coupling λ, list of mass modifications $\{\alpha_i\}$, upper pullback bound r_{max}, resolution res
Output: Interval $[r_{\text{lower}}, r_{\text{upper}}]$ estimating critical pullback r_c for each α_i
for each α in $\{\alpha_0, \alpha_1, \dots\}$ **do**
    Set initial bounds: $r_{\text{lower}} \leftarrow 0$ and $r_{\text{upper}} \leftarrow r_{\text{max}}$
    while $|r_{\text{upper}} - r_{\text{lower}}| >$ res **do**
        $r \leftarrow \frac{1}{2}(r_{\text{lower}} + r_{\text{upper}})$ ▷ Bisect current interval
        $n \leftarrow$ GetNumberOfRelevantThimbles$(\sigma, \lambda, r, \alpha)$
        if $n = 1$ **then**
            $r_{\text{upper}} \leftarrow r$ ▷ r_c is below current r
        else
            $r_{\text{lower}} \leftarrow r$ ▷ r_c is above current r
        end if
    end while
    Store $[\alpha, r_{\text{lower}}, r_{\text{upper}}, \sigma, \lambda]$
end for

σ	r_c	α_c
$-4+1i$	56.88	0.72
$-3+1i$	15.49	0.89
$-2+1i$	11.24	0.94
$-1+1i$	3.81	2.89
$-1+2i$	6.46	1.44
$-1+3i$	12.23	1.11
$-1+4i$	19.12	1.22

(a) $\text{Re}(\sigma) < 0$

σ	r_c	α_c
$+1+4i$	5.20	1.75
$+1+3i$	3.38	2.06
$+1+2i$	2.20	2.22
$+1+1i$	2.26	1.35

(b) $\text{Re}(\sigma) > 0$

Tab. 4.3: Critical parameters that separate the multi-thimble regime from the single-thimble regime in the (r, α) plane with $\lambda = 2$. The critical parameters with the minimal pullback r are given. In the regime $(r > r_c, \alpha_c)$, we expect to see a single relevant thimble.

4.4 Recovery of observables via bias correction

Having established that an additive modification of the action can deform the Lefschetz thimble structure towards a single relevant thimble, we now analyze whether observables of the unmodified theory can be recovered from simulations performed in the modified theory. This is achieved by

Die approbierte gedruckte Originalversion dieser Diplomarbeit ist an der TU Wien Bibliothek verfügbar
The approved original version of this thesis is available in print at TU Wien Bibliothek.
TU Bibliothek Your knowledge hub WIEN

using the bias correction scheme outlined in Section 4.2. As discussed there, the expectation values obtained in the modified theory generally differ from those in the original theory due to the modified weight in the path integral. However, by leveraging analytic knowledge of an observable that vanishes in the unmodified theory, we compute a correction factor Q (Eq. (4.21)), which can then be used to recover the original values of the observables from modified simulations. In what follows, we used the observable $\mathcal{O}_1^* = 1 - \phi(\sigma\phi + \lambda\phi^3)$ with the key property $\langle \mathcal{O}_1^* \rangle_\rho = 0$ to determine the correction weight Q using CL simulations in the modified theory.

We summarize our results of the first and second moment in Tables 4.4, 4.5 and 4.6 and compare them to numerical values determined by a quadrature routine. Table 4.4 presents the first moment $\langle\phi\rangle$, determined by CL with respect to the modified weight. There, we also show the modification parameters (r, α) used to obtain these results. As expected, the $\mathbb{Z}_2$ symmetry stays preserved after the modification, and the analytical value of the first moment yields zero. The results obtained by CL are consistent with zero within the first three digits for all tested values of σ, including those deep in the broken phase. In Table 4.5 we show the CL results of the second moment $\langle\phi^2\rangle$ obtained for the modified theory as well as the modification parameters. Here we observe a significant improvement over the unmodified CL results presented in section 4.1; the results show good agreement with the numerical values, even in the phase of broken symmetry. We attribute this improvement to the successful suppression of multi-thimble interference by the modification, leading to correct CL convergence in the modified case.

However, the modification that we applied to restore a unique thimble structure shifts the expectation values away from the original theory. In order to reconstruct these observables, we apply the bias correction scheme discussed in section 4.2. The bias corrected results obtained for the second moment are shown in Table 4.6. Using the bias correction method, we were able to reconstruct the second moment for all the mass parameters tested. Both real and imaginary parts of $\langle\phi^2\rangle$ match the numerical predictions within a few significant digits, confirming the validity and precision of the correction strategy. Notably, the bias correction works even in regimes where the unmodified CL method fails dramatically. For example, for $\sigma = -4 + 1i$, the unmodified method yields a second moment that differs by nearly a factor of 5, while the corrected result aligns with the exact value to better than 1%.

We note that the results presented in Tables 4.4, 4.5 and 4.6 do not give correct results within the statistical significance for all choices of σ. This we attribute to a discretization artifact due to a finite Langevin stepsize. Another potential issue is the fact that real and imaginary parts are, in general, not uncorrelated. To give a more precise error estimate, one would have to propagate the correlated error through the bias correction scheme.

Figure 4.3 shows how the CL process samples close to the relevant thimble if there is a single relevant one (for a sufficiently strong $r > r_c$, shown in the upper panel) and spreads out in the case of multiple relevant thimbles (when $r < r_c$, shown in the middle panel). It also displays in the lower panel how the correctness criterion on the drift magnitude distribution is validated in the single thimble regime ($r > r_c$) and violated in the regime where multiple thimbles are relevant ($r < r_c$). These results conclusively demonstrate the following:

- The Gaussian modification (4.22) succeeds in isolating a single relevant thimble for an appropriate choice of modification parameters.
- The CL process in the modified theory converges reliably.
- The bias introduced by the modification can be accurately corrected.

Altogether, this constitutes a robust framework for restoring CL convergence by thimble-based density modifications, offering a promising route for applying CL to more complex theories with severe sign problems.

Die approbierte gedruckte Originalversion dieser Diplomarbeit ist an der TU Wien Bibliothek verfügbar
The approved original version of this thesis is available in print at TU Wien Bibliothek.
TU Bibliothek Your knowledge hub WIEN

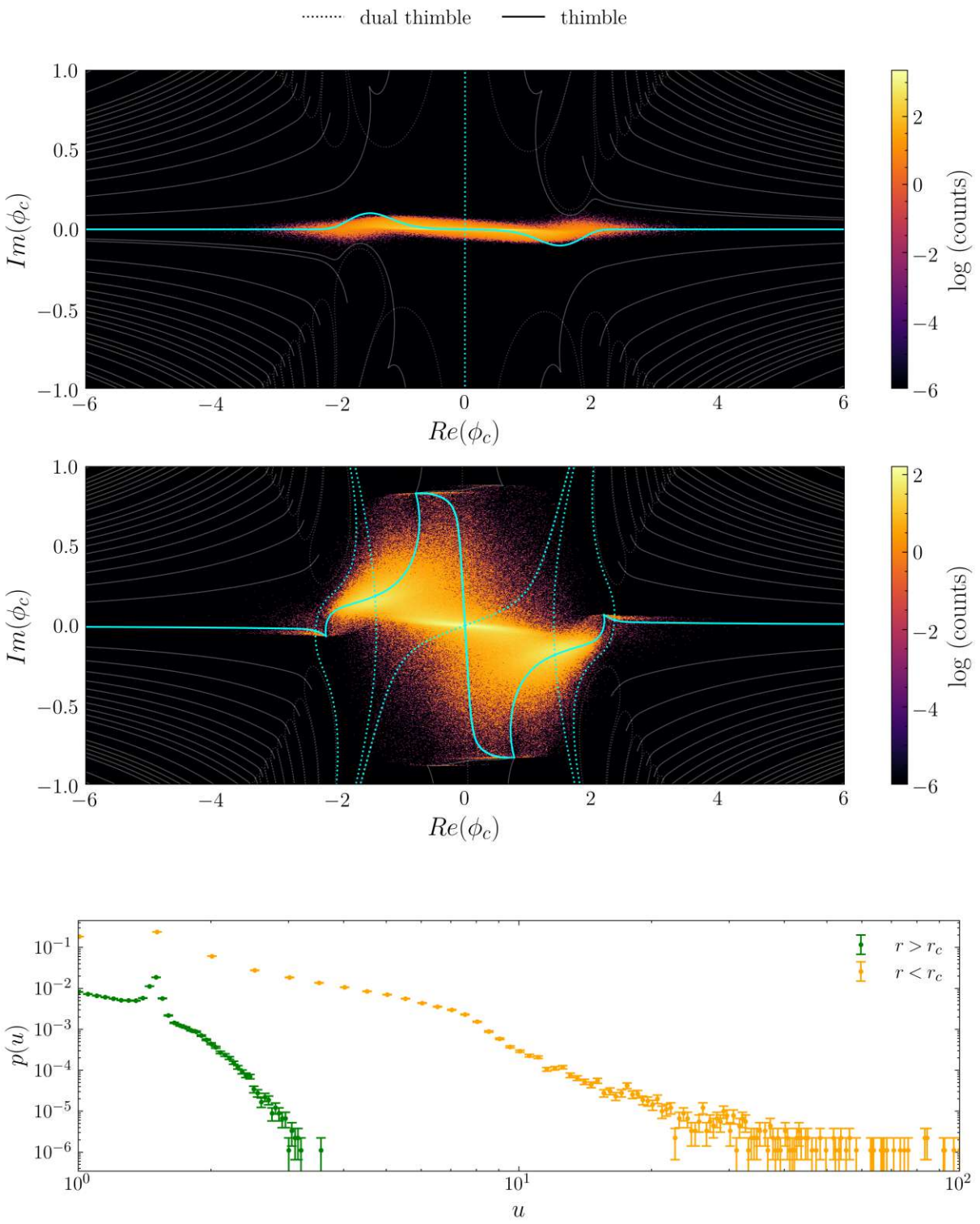

Fig. 4.3: CL sampling densities overlaid on Lefschetz thimbles for the modified theory with $\lambda = 2$ and $\sigma = -4 + i$. Top: For $r > r_c$, only one thimble contributes and CL dynamics remain localized close to the relevant thimble, leading to correct convergence. Middle: For $r < r_c$, multiple thimbles are relevant and CL explores a wider region, causing wrong convergence. Bottom: Corresponding drift histograms. The correctly converging case shows rapid decay, while the incorrect case exhibits a long tail, violating the drift-based correctness criterion (see Chapter 2.3.2).

Die approbierte gedruckte Originalversion dieser Diplomarbeit ist an der TU Wien Bibliothek verfügbar
The approved original version of this thesis is available in print at TU Wien Bibliothek.

σ	$\mathrm{Re}\langle\phi\rangle_{\tilde{\rho}}^{\mathrm{CL}}$	$\mathrm{Re}\langle\phi\rangle_{\tilde{\rho}}^{\mathrm{exact}}$	$\mathrm{Im}\langle\phi\rangle_{\tilde{\rho}}^{\mathrm{CL}}$	$\mathrm{Im}\langle\phi\rangle_{\tilde{\rho}}^{\mathrm{exact}}$	α	r
$-4+1i$	0.000120(4)	0	0.000008(4)	0	0.72	227.52
$-3+1i$	0.000115(4)	0	0.000007(4)	0	0.89	61.95
$-2+1i$	0.000120(2)	0	0.000003(2)	0	0.94	44.97
$-1+1i$	0.000095(5)	0	−0.000000(5)	0	2.89	15.62
$-1+3i$	0.000112(2)	0	0.000000(2)	0	1.11	49.06
$-1+2i$	0.000106(3)	0	−0.000001(3)	0	1.42	25.75
$-1+4i$	0.000109(1)	0	−0.000000(1)	0	1.22	76.56
$+1+4i$	−0.000065(2)	0	0.000002(2)	0	1.75	20.80
$+1+3i$	−0.000048(3)	0	0.000003(3)	0	2.06	13.52
$+1+2i$	−0.000042(3)	0	0.000005(3)	0	2.22	8.80
$+1+1i$	−0.000093(2)	0	0.000004(2)	0	1.35	9.04

Tab. 4.4: Comparison of $\langle\phi\rangle$ between CL and exact results, with mass modification and pullback.

σ	$\mathrm{Re}\langle\phi^2\rangle_{\tilde{\rho}}^{\mathrm{CL}}$	$\mathrm{Re}\langle\phi^2\rangle_{\tilde{\rho}}^{\mathrm{exact}}$	$\mathrm{Im}\langle\phi^2\rangle_{\tilde{\rho}}^{\mathrm{CL}}$	$\mathrm{Im}\langle\phi^2\rangle_{\tilde{\rho}}^{\mathrm{exact}}$	α	r
$-4+1i$	1.349237(9)	1.349110	−0.011159(9)	−0.011165	0.72	227.52
$-3+1i$	1.161145(9)	1.161019	−0.012971(9)	−0.012978	0.89	61.95
$-2+1i$	1.227474(5)	1.227346	−0.002930(5)	−0.002937	0.94	44.97
$-1+1i$	0.366643(7)	0.366534	−0.027749(7)	−0.027743	2.89	15.62
$-1+2i$	0.686013(5)	0.685878	−0.007997(5)	−0.007998	1.42	25.75
$-1+3i$	0.888077(4)	0.887937	0.001526(4)	0.001522	1.11	49.06
$-1+4i$	0.811462(2)	0.811321	0.002345(2)	0.002343	1.22	76.56
$+1+4i$	0.556382(3)	0.556334	0.000918(3)	0.000917	1.75	20.80
$+1+3i$	0.466796(4)	0.466743	−0.004562(4)	−0.004565	2.06	13.52
$+1+2i$	0.431590(4)	0.431534	−0.010721(4)	−0.010722	2.22	8.80
$+1+1i$	0.708387(3)	0.708350	−0.001862(3)	−0.001863	1.35	9.04

Tab. 4.5: Comparison of $\langle\phi^2\rangle$ between CL and exact results, with mass modification and pullback.

σ	$\mathrm{Re}\langle\phi^2\rangle_{\tilde{\rho}}^{\text{bias corr}}$	$\mathrm{Re}\langle\phi^2\rangle_{\rho}^{\mathrm{exact}}$	$\mathrm{Im}\langle\phi^2\rangle_{\tilde{\rho}}^{\text{bias corr}}$	$\mathrm{Im}\langle\phi^2\rangle_{\rho}^{\mathrm{exact}}$	α	r
$-4+1i$	1.68(4)	1.67	−0.5132(2)	−0.5111	0.72	227.52
$-3+1i$	1.191(9)	1.190	−0.413(5)	−0.411	0.89	61.95
$-2+1i$	0.8390(8)	0.8394	−0.296(5)	−0.294	0.94	44.97
$-1+1i$	0.604(2)	0.605	−0.1983(6)	−0.1983	2.89	15.62
$-1+2i$	0.485(1)	0.485	−0.366(4)	−0.365	1.43	25.75
$-1+3i$	0.300(8)	0.301	−0.46(1)	−0.46	1.11	49.06
$-1+4i$	0.10(2)	0.11	−0.45(2)	−0.44	1.22	76.56
$1+4i$	0.158(2)	0.159	−0.2235(9)	−0.2230	20.80	1.75
$1+3i$	0.2317(8)	0.2320	−0.2092(6)	−0.2090	13.52	2.06
$1+2i$	0.30034(2)	0.30048	−0.1628(5)	−0.1626	8.8	2.22
$1+1i$	0.3485(8)	0.3487	−0.0890(3)	−0.0889	9.04	1.35

Tab. 4.6: Comparison of $\langle\phi^2\rangle$ between the bias corrected results obtained CL and exact results, with mass modification and pullback.

Die approbierte gedruckte Originalversion dieser Diplomarbeit ist an der TU Wien Bibliothek verfügbar
The approved original version of this thesis is available in print at TU Wien Bibliothek.
TU Bibliothek Your knowledge hub WIEN

Chapter 5

Conclusion and Outlook

In this thesis, we investigated the Lefschetz thimble structure of a scalar model in zero dimensions and examined its relationship with the convergence behavior of the complex Langevin (CL) method. Motivated by the sign problem inherent in quantum field theories with complex actions, we explored a strategy to improve—or even remedy—the convergence properties of CL by leveraging insights from thimble geometry.

We began by formulating a real scalar model with a single degree of freedom and analytically continued the action into the complexified field space. This enabled the application of Picard–Lefschetz theory, which associates each saddle point of the complexified action with a corresponding Lefschetz thimble — a manifold along which the path integral can be evaluated with a real and positive weight. This geometric decomposition offers a powerful alternative perspective to stochastic quantization. The CL method evolves field configurations through the complexified space according to a set of stochastic differential equations. Despite its ability to bypass the sign problem in certain regimes, CL is known to suffer from convergence failures, including incorrect results in some parameter regions and the presence of runaway trajectories. A major objective of this thesis was to examine these shortcomings from the viewpoint of the underlying thimble structure.

Our numerical investigations revealed a strong correlation between CL convergence and the number of relevant thimbles. When a single thimble associated with an attractive critical point dominates, the CL process usually samples configurations such that the criteria for correctness are satisfied. Exceptions in the unmodified theory are pointed out in [40]. In these cases, the distribution of large drift magnitudes — a quantity proportional to the field update per Langevin time step — is suppressed more strongly than any polynomial, in agreement with formal convergence theorems. We observed that CL fails to produce correct results in the broken-symmetry phase and near the phase transition. Moreover, at the symmetry-breaking point, multiple thimbles become relevant, signaling a breakdown in the conditions required for CL to converge reliably.

Building on the geometric analysis, we introduced an additive density modification aimed at isolating a single relevant thimble. This approach was originally developed to restore convergence in models defined on compact domains. In this work, we adapted the technique to a theory defined on a non-compact domain. We demonstrated that the bias introduced by the modification can itself be estimated using CL in the regime where a single thimble is dominant, thus preserving the overall correctness of observables.

This work opens several avenues for further research. First, extending the analysis to higher-dimensional field theories would provide a more realistic setting to test the interplay between CL dynamics and thimble geometry. A deeper understanding of the thimble landscape could guide the construction of kernels or reweighting schemes to improve CL convergence in such systems. Second, the role of Stokes phenomena—transitions in the set of contributing thimbles as parameters vary—requires further study. In particular, our results suggest that the single-thimble criterion is not strictly sufficient to ensure correct convergence near critical points such as the

Die approbierte gedruckte Originalversion dieser Diplomarbeit ist an der TU Wien Bibliothek verfügbar
The approved original version of this thesis is available in print at TU Wien Bibliothek.
TU Bibliothek Your knowledge hub WIEN

symmetry-breaking transition. This conclusion is supported by earlier observations that CL can converge incorrectly even in the presence of a single relevant thimble [40]. However, we have shown that in such cases, density modifications can still improve the convergence behavior of the CL method. This indicates that a more refined set of correctness conditions, possibly incorporating the structure of the drift, the presence of poles, and the decay behavior in complex directions, may be necessary to fully characterize the validity of CL.

Die approbierte gedruckte Originalversion dieser Diplomarbeit ist an der TU Wien Bibliothek verfügbar
The approved original version of this thesis is available in print at TU Wien Bibliothek.
TU Bibliothek Your knowledge hub WIEN

Bibliography

[1] K. Boguslavski, P. Hotzy, and D. I. Müller, "Real-time correlators in 3+1D thermal lattice gauge theory," *Phys. Rev. D* **109** no. 9, (2024) 94518.

[2] C. Bonati, M. D'Elia, P. Rossi, and E. Vicari, "θ dependence of 4D SU(N) gauge theories in the large-N limit," *Phys. Rev. D* **94** no. 8, (2016) 85017.

[3] G. Aarts, L. Bongiovanni, E. Seiler, D. Sexty, and I.-O. Stamatescu, "Controlling complex Langevin dynamics at finite density," *Eur. Phys. J. A* **49** (2013) 89.

[4] M. Unsal, "Theta dependence, sign problems and topological interference," *Phys. Rev. D* **86** (2012) 105012.

[5] P. de Forcrand, "Simulating QCD at finite density," *PoS* **LAT2009** (2009) 10.

[6] K. Nagata, "Finite-density lattice QCD and sign problem: Current status and open problems," *Prog. Part. Nucl. Phys.* **127** (2022) 103991.

[7] M. C. Bañuls and K. Cichy, "Review on Novel Methods for Lattice Gauge Theories," *Rept. Prog. Phys.* **83** no. 2, (2020) 24401.

[8] G. Parisi, "ON COMPLEX PROBABILITIES," *Phys. Lett. B* **131** (1983) 393–395.

[9] G. Aarts, F. A. James, E. Seiler, and I.-O. Stamatescu, "Complex Langevin: Etiology and Diagnostics of its Main Problem," *Eur. Phys. J. C* **71** (2011) 1756.

[10] C. E. Berger, L. Rammelmüller, A. C. Loheac, F. Ehmann, J. Braun, and J. E. Drut, "Complex Langevin and other approaches to the sign problem in quantum many-body physics," *Physics Reports* **892** (2021) 1–54.

[11] J. R. Klauder, "Coherent State Langevin Equations for Canonical Quantum Systems With Applications to the Quantized Hall Effect," *Phys. Rev. A* **29** (1984) 2036–2047.

[12] G. Aarts and I.-O. Stamatescu, "Stochastic quantization at finite chemical potential," *JHEP* **09** (2008) 18.

[13] G. Aarts, "Complex Langevin dynamics and other approaches at finite chemical potential," *PoS* **LATTICE2012** (2012) 17.

[14] E. Witten, "Analytic Continuation Of Chern-Simons Theory," *AMS/IP Stud. Adv. Math.* **50** (2011) 347–446.

[15] M. Cristoforetti, L. Scorzato, and F. Di Renzo, "The sign problem and the Lefschetz thimble," *J. Phys. Conf. Ser.* **432** (2013) 12025.

[16] G. Parisi and Y. WU, "Pertubation theory without gauge fixing," *Scientia Sinica* **24** no. 4, (1981) .

Die approbierte gedruckte Originalversion dieser Diplomarbeit ist an der TU Wien Bibliothek verfügbar
The approved original version of this thesis is available in print at TU Wien Bibliothek.
TU Bibliothek Your knowledge hub WIEN

[17] G. Aarts, E. Seiler, and I. O. Stamatescu, "Complex Langevin method: When can it be trusted?," *Phys. Rev. D* **81** no. 5, (3, 2010) .

[18] S. Tsutsui and T. M. Doi, "Improvement in complex Langevin dynamics from a view point of Lefschetz thimbles," *Phys. Rev. D* **94** no. 7, (2016) 74009.

[19] J. Nishimura and S. Shimasaki, "Combining the complex Langevin method and the generalized Lefschetz-thimble method," *JHEP* **06** (2017) 23.

[20] G. Aarts, L. Bongiovanni, E. Seiler, and D. Sexty, "Some remarks on Lefschetz thimbles and complex Langevin dynamics," *JHEP* **10** (2014) 159.

[21] K. Boguslavski, P. Hotzy, and D. I. Müller, "Lefschetz thimble-inspired weight regularizations for complex Langevin simulations," *SciPost Phys.* **18** (2025) 92.

[22] T. Hayata, Y. Hidaka, and Y. Tanizaki, "Complex saddle points and the sign problem in complex Langevin simulation," *Nucl. Phys. B* **911** (2016) 94–105.

[23] G. Aarts, "Lefschetz thimbles and stochastic quantization: Complex actions in the complex plane," *Phys. Rev. D* **88** no. 9, (2013) 94501.

[24] S. Tsutsui and T. M. Doi, "On a modification method of Lefschetz thimbles," *EPJ Web Conf.* **175** (2018) 11016.

[25] A. Kumar, A. Joseph, and P. Kumar, "Complex Langevin Study of Spontaneous Symmetry Breaking in IKKT Matrix Model," *PoS* **LATTICE2022** (2023) 213.

[26] C. Pehlevan and G. Guralnik, "Complex Langevin Equations and Schwinger-Dyson Equations," *Nucl. Phys. B* **811** (2009) 519–536.

[27] R. M. Munasinghe, "Closed-Form Solutions of Zero Dimensional ϕˆ4-Field Theory Using Bessel Functions: A Non-Perturbative Approach," *Heliyon* **9** (5, 2022) e13168.

[28] D. Alvestad, A. Rothkopf, and D. Sexty, "Real time simulations of scalar fields with kernelled complex Langevin equation," in *41st International Symposium on Lattice Field Theory*. 5, 2025.

[29] R. Bharathkumar and A. Joseph, "Lefschetz Thimbles and Quantum Phases in Zero-Dimensional Bosonic Models," *Eur. Phys. J. C* **80** no. 10, (2020) 923.

[30] R. MacKenzie, "Path integral methods and applications," in *6th Vietnam International School on Physics*. 5, 1999.

[31] G. Cohen, E. Gull, D. R. Reichman, and A. J. Millis, "Taming the dynamical sign problem in real-time evolution of quantum many-body problems," *Physical Review Letters* **115** no. 26, (10, 2015) .

[32] K. Binder, ed., *MONTE CARLO METHODS IN STATISTICAL PHYSICS*, vol. 7 of *Topics in Current Physics*. Springer-Verlag, Berlin, Germany, 1986.

[33] C. Gattringer, "New developments for dual methods in lattice field theory at non-zero density," *PoS* **LATTICE2013** (2014) 2.

[34] C. Gattringer and K. Langfeld, "Approaches to the sign problem in lattice field theory," *Int. J. Mod. Phys. A* **31** no. 22, (2016) 1643007.

Die approbierte gedruckte Originalversion dieser Diplomarbeit ist an der TU Wien Bibliothek verfügbar
The approved original version of this thesis is available in print at TU Wien Bibliothek.
TU Bibliothek Your knowledge hub WIEN

[35] N. Prokof'ev and B. Svistunov, "Worm Algorithms for Classical Statistical Models," *Phys. Rev. Lett.* **87** (2001) 160601.

[36] M. Brics, J. Kaupužs, and R. Mahnke, "How to solve Fokker-Planck equation treating mixed eigenvalue spectrum?," *Condensed Matter Physics* **16** no. 1, (2013) 1–13.

[37] T. Szabados, "An elementary introduction to the Wiener process and stochastic integrals," *Studia Scientiarum Mathematicarum Hungarica* **31** (5, 2010) .

[38] H. Risken and H. Haken, *The Fokker-Planck Equation: Methods of Solution and Applications Second Edition*, vol. 18. Springer-Verlag, 2 ed., 1996.

[39] H. Nakazato and Y. Yamanaka, "MINKOWSKI STOCHASTIC QUANTIZATION," *Phys. Rev. D* **34** (1986) 492.

[40] P. Giudice, G. Aarts, and E. Seiler, "Localised distributions in complex Langevin dynamics," *PoS* **LATTICE2013** (2014) 200.

[41] A. Mollgaard and K. Splittorff, "Complex Langevin Dynamics for chiral Random Matrix Theory," *Phys. Rev. D* **88** no. 11, (2013) 116007.

[42] Y. Ito and J. Nishimura, "The complex Langevin analysis of spontaneous symmetry breaking induced by complex fermion determinant," *JHEP* **12** (2016) 9.

[43] G. Aarts, E. Seiler, D. Sexty, and I.-O. Stamatescu, "Complex Langevin dynamics and zeroes of the fermion determinant," *JHEP* **05** (2017) 44.

[44] G. Aarts and F. A. James, "Complex Langevin dynamics in the SU(3) spin model at nonzero chemical potential revisited," *JHEP* **01** (2012) 118.

[45] E. Seiler, D. Sexty, and I.-O. Stamatescu, "Gauge cooling in complex Langevin for QCD with heavy quarks," *Phys. Lett. B* **723** (2013) 213–216.

[46] J. Nishimura and S. Shimasaki, "New Insights into the Problem with a Singular Drift Term in the Complex Langevin Method," *Phys. Rev. D* **92** no. 1, (2015) 11501.

[47] K. Nagata, J. Nishimura, and S. Shimasaki, "The argument for justification of the complex Langevin method and the condition for correct convergence," *Phys. Rev. D* **94** no. 11, (2016) 114515.

[48] K. Nagata, J. Nishimura, and S. Shimasaki, "Testing the criterion for correct convergence in the complex Langevin method," *JHEP* **05** (2018) 4.

[49] E. Seiler, D. Sexty, and I.-O. Stamatescu, "Complex Langevin: Correctness criteria, boundary terms, and spectrum," *Phys. Rev. D* **109** no. 1, (2024) 14509.

[50] E. Seiler, "Complex Langevin: Boundary Terms at Poles of the drift," *PoS* **LATTICE2021** (2022) 210.

[51] E. Witten, "A New Look At The Path Integral Of Quantum Mechanics," *Surveys in Differential Geometry* **15** (5, 2010) 345–419.

[52] T. Kanazawa and Y. Tanizaki, "Structure of Lefschetz thimbles in simple fermionic systems," *JHEP* **03** (2015) 44.

Die approbierte gedruckte Originalversion dieser Diplomarbeit ist an der TU Wien Bibliothek verfügbar
The approved original version of this thesis is available in print at TU Wien Bibliothek.
TU Bibliothek Your knowledge hub WIEN

[53] M. W. Hansen, M. Mandl, E. Seiler, and D. Sexty, "Role of integration cycles in complex Langevin simulations," *Phys. Rev. D* **111** no. 7, (2025) 74502.

[54] L. L. Salcedo and E. Seiler, "SchwingerDyson equations and line integrals," *J. Phys. A* **52** no. 3, (2019) 35201.

[55] "Chapter 4 Morse Theory," in *Comparison Theorems in Riemannian Geometry*, J. Cheeger and D. G. Ebin, eds., vol. 9 of *North-Holland Mathematical Library*, pp. 80–92. Elsevier, 1975.

[56] K. Boguslavski, P. Hotzy, and D. I. Müller, "Stabilizing complex Langevin for real-time gauge theories with an anisotropic kernel," *JHEP* **06** (2023) 11.

[57] J. Flower, S. W. Otto, and S. Callahan, "Complex Langevin Equations and Lattice Gauge Theory," *Phys. Rev. D* **34** (1986) 598.

[58] G. Aarts, F. A. James, E. Seiler, and I.-O. Stamatescu, "Adaptive stepsize and instabilities in complex Langevin dynamics," *Phys. Lett. B* **687** (2010) 154–159.

[59] B. A. Berg, *Introduction to Markov chain Monte Carlo simulations and their statistical analysis.* World Scientific, 5, 2004.

[60] D. Alvestad, R. Larsen, and A. Rothkopf, "Towards learning optimized kernels for complex Langevin," *JHEP* **04** (2023) 57.

[61] M. Mandl, M. W. Hansen, E. Seiler, and D. Sexty, "Kernels and integration cycles in complex Langevin simulations," *PoS* **LATTICE2024** (2025) 59.

Die approbierte gedruckte Originalversion dieser Diplomarbeit ist an der TU Wien Bibliothek verfügbar
The approved original version of this thesis is available in print at TU Wien Bibliothek.
TU Bibliothek Your knowledge hub WIEN